ELSEVIER

Journal of Structural Geology 29 (2007) 1722–1743

JOURNAL OF STRUCTURAL GEOLOGY

www.elsevier.com/locate/jsg

Microstructural-deformation record of an orogen-parallel extension in the Vepor Unit, West Carpathians

Petr Jeřábek [a,b,*], Holger Stünitz [c], Renée Heilbronner [c], Ondrej Lexa [a,d], Karel Schulmann [d]

[a] *Institute of Petrology and Structural Geology, Charles University, Albertov 6, 128 43 Prague, Czech Republic*
[b] *Czech Geological Survey, Klárov 3, 118 21 Praha 1, Czech Republic*
[c] *Geologisch-Paläontologisches Institut, Universität Basel, 4056 Basel, Switzerland*
[d] *Université Louis Pasteur, EOST, UMR 7517, 1 Rue Blessig, Strasbourg 67084, France*

Received 21 June 2007; received in revised form 5 September 2007; accepted 6 September 2007
Available online 20 September 2007

Abstract

Deformation microstructures of quartzo-feldspathic rocks have been used to analyse the orogen-parallel stretching of the Vepor Unit in the West Carpathians during Cretaceous convergence. This process occurs contemporaneously with the burial of the Vepor basement related to the overthrusting Palaeozoic volcano-sedimentary sequences of the Gemer Unit. The microstructures develop along a metamorphic gradient indicating an increase of pressure and temperature towards the structural footwall. The recrystallization of quartz occurs in the field of subgrain rotation recrystallization (SGR) while the plagioclase and K-feldspar disintegrate into a neocrystallized muscovite-albite matrix. Palaeopiezometry of the recrystallized quartz in conjunction with P–T estimates yield strain rates of 9×10^{-12} to 6×10^{-14} s^{-1}, depending on temperature (380–480 °C) and choice of piezometer and flow law calibration. Strain analysis of the recrystallized quartz aggregates and quartz texture analysis indicate an overprint of the Variscan magmatic and high grade fabrics by a Cretaceous plane strain deformation resulting in vertical shortening and horizontal orogen parallel East–West stretching. Spatial distribution and conflicting sense-of-shear of the asymmetrical quartz lattice preferred orientation patterns indicate that the large-scale pure shear deformation of the Vepor Unit is locally accommodated by simple shear zones. Observed metamorphic gradients across the Vepor Unit are interpreted to result from later large-scale folding and heterogeneous exhumation of the orogen-parallel deformation fabric.

Keywords: Crustal stresses and strain rates; Orogen-parallel extension; Quartz deformation microstructures and textures; Microstructure of quartzo-feldspathic rocks; West Carpathians

1. Introduction

Microstructures of quartzo-feldspathic rocks consisting mostly of quartz, feldspars and micas may be used to characterize the deformation processes of mid-crustal rocks as such rocks are abundant at these crustal levels. This is made possible due to number of experimental as well as natural studies on single phase deformation microstructures and rheological behaviour of quartz (Hirth and Tullis, 1992; Hirth et al., 2001; Stipp et al., 2002a,b), of plagioclase (Tullis and Yund, 1985; Kruse et al., 2001; Stünitz et al., 2003) and of micas (Shea and Kronenberg, 1993; Mares and Kronenberg, 1993; Mariani et al., 2006).

Among these minerals, the rheological properties of quartz are the best constrained and most predictable, which, together with its abundance and relative mechanical weakness, makes quartz an ideal mineral to estimate the rheology of the middle crust. By analysing the quartz deformation microstructure and texture it is possible to derive approximate deformation temperatures (Stipp et al., 2002b), differential stresses (Twiss, 1977; Koch, 1983; Stipp and Tullis, 2003), type of strain

* Corresponding author: Institute of Petrology and Structural Geology, Charles University, Albertov 6, 128 43 Prague, Czech Republic. Tel.: +420 2 2195 1534.
E-mail address: jerabek1@natur.cuni.cz (P. Jeřábek).

0191-8141/$ - see front matter © 2007 Elsevier Ltd. All rights reserved.
doi:10.1016/j.jsg.2007.09.002

(Lister and Hobbs, 1980; Schmid and Casey, 1986) and deformation kinematics (Simpson and Schmid, 1983). In the context of regional studies, however, the analyses of quartz deformation were mostly concentrated on differential stresses, strain rates and crustal viscosities (Hacker et al., 1990, 1992; Dunlap et al., 1997; Lobkowicz et al., 1998; Stöckhert et al., 1999; Zulauf, 2001). Recent advances in the techniques of quartz microstructure and texture analysis allow an acquisition of large datasets, which may significantly improve our understanding of mechanics of the large scale tectonic processes (Kurz et al., 2001, 2002; Stipp et al., 2004). In this contribution we concentrate on quartz and plagioclase fabrics developed during the Upper Cretaceous deformation of quartzo-feldspathic basement rocks of the Vepor Unit in the West Carpathians.

2. Geological setting

The Central West Carpathians (Fig. 1) consist of three major crustal units – Gemer, Vepor and Tatra – composed of Variscan basement and Late Palaeozoic-Mesozoic metasedimentary cover. The southern Gemer Unit consists of Lower Palaeozoic volcano-sedimentary sequences affected by Variscan low/medium grade metamorphism (Faryad, 1991) and Carboniferous–Triassic cover. Basement and cover of this unit are tectonically overlain by Jurassic subduction-accretionary complex of the Meliata Ocean (Faryad, 1995; Faryad and Henjes-Kunst, 1997). The central Vepor Unit and the northern Tatra Unit are composed of Variscan medium/high grade metamorphic rocks, Carboniferous granitoids and Permian–Cretaceous cover. During Jurassic and Early Cretaceous the Vepor and Tatra Units were separated by the so called Fatric domain, consisting of thinned basement and associated sedimentary basin (Krížna). Cretaceous convergence led to the South to North welding of the three main units and to overthrusting of the Late Palaeozoic–Lower Cretaceous platform and rift-related sedimentary sequences of the Krížna, Choč, Turňa and Silica nappes (cf. Plašienka et al., 1997; Fig. 1). As a result, the three main crustal units were stacked in the following structural order from top to bottom, i.e., from South to North (Fig. 2): (i) the Gemer Unit; (ii) the Vepor Unit; and (iii) the Tatra Unit (e.g. Tomek, 1993; Lexa et al., 2003; Plašienka, 2003). Cretaceous deformation and metamorphic overprint is seen as lower greenschist to greenschist facies in the Gemer Unit (Faryad, 1997; Petrasová et al., 2007), upper greenschist/amphibolite facies in the Vepor Unit (Vrána, 1980; Janák et al., 2001; Koroknai et al., 2001; Jeřábek et al., in press) and prehnite-pumpellyite facies in the northern Tatra Unit (Krist et al., 1992).

2.1. Vepor Unit

The overall structure of the Vepor Unit is characterized by an alternation of NE–SW trending belts with different lithological content (Fig. 1). The basement is divided into two complexes following the dominant lithology and structural position (Klinec, 1966). The structurally lower Hron Complex (Fig. 2) is formed by paragneisses, micaschists and amphibolites, which record Variscan and Alpine metamorphism (Maluski et al., 1993; Kováčik et al., 1996; Král' et al., 1996) reaching the staurolite/kyanite zone during both events (Méres and Hovorka, 1991; Kováčik et al., 1996; Jeřábek et al., in press). The structurally higher Král'ova Hol'a Complex is formed by Late Devonian migmatites and anatectic orthogneisses, and several large intrusive bodies of Lower Carboniferous S-type granitoids and Upper-Carboniferous tonalites (Bibikova et al., 1988, 1990; Michalko et al., 1998). The migmatites and anatectic orthogneisses have reached conditions of partial melting during the Variscan and have been reworked in greenschist facies during the Alpine event (Siman et al., 1996), while the Late Variscan granitoids are only affected by the greenschist facies Alpine metamorphism (Vrána, 1980; Jeřábek et al., in press). The division of the Vepor basement into two litho-tectonic complexes (Klinec, 1966) was later questioned mostly due to the differences in lithology and degree of Alpine tectono-metamorphic reworking of the southern and northern part of the Hron Complex (Fig. 1). Nevertheless, the mutual structural relationship of the two dominant lithologies within the Vepor Unit is identical to that of the Tatra Unit and that of the eastern segment of the Vepor Unit (Fig. 1), exhibiting lower degree of Alpine reworking (Janák, 1994; Jacko et al., 1996). Consequently, the inverted crustal structure (granitoids overlying metasediments) within both units argues for an inherited Variscan crustal stratification (Bezák et al., 1997). The southern rim of the Vepor basement (Gemer/Vepor Contact Zone) consists of schists, which have reached upper greenschist/amphibolite facies conditions during the Variscan as well as the Alpine event (Lupták et al., 2000; Jeřábek et al., in press).

Two metamorphosed cover successions with distinct lithostratigraphic content are recognised in the Vepor Unit (Biely, 1964). The Permo-Triassic para-autochthonous Foederata Cover overlies basement rocks of the southern, eastern and central part of the Vepor Unit (Fig. 1) whereas the Permian to Lower Cretaceous allochthonous Vel'ký Bok Cover is present at the northern edge of the Vepor Unit. Alpine metamorphism indicates very low-grade metamorphism in the Vel'ký Bok Cover and lower greenschist facies conditions in the Foederata Cover (Lupták et al., 2003).

3. Structural record

Three main deformation events were identified in the Variscan basement of the Vepor Unit and two in the Permian to Lower Cretaceous cover (Fig. 2). The earliest deformation event denoted as D_V records Variscan deformation and affects only the Vepor basement. The later two deformation events, affecting both the basement and cover, are related to the first and second Alpine deformation events denoted as D_{A1} and D_{A2}.

The earliest deformation event D_V has produced a high grade metamorphic schistosity S_V in the paragneisses-micaschists of the Hron Complex and in the schists of the southern Gemer/Vepor Contact Zone, and a high grade orthogneiss fabric and migmatite layering in the Král'ova Hol'a Complex.

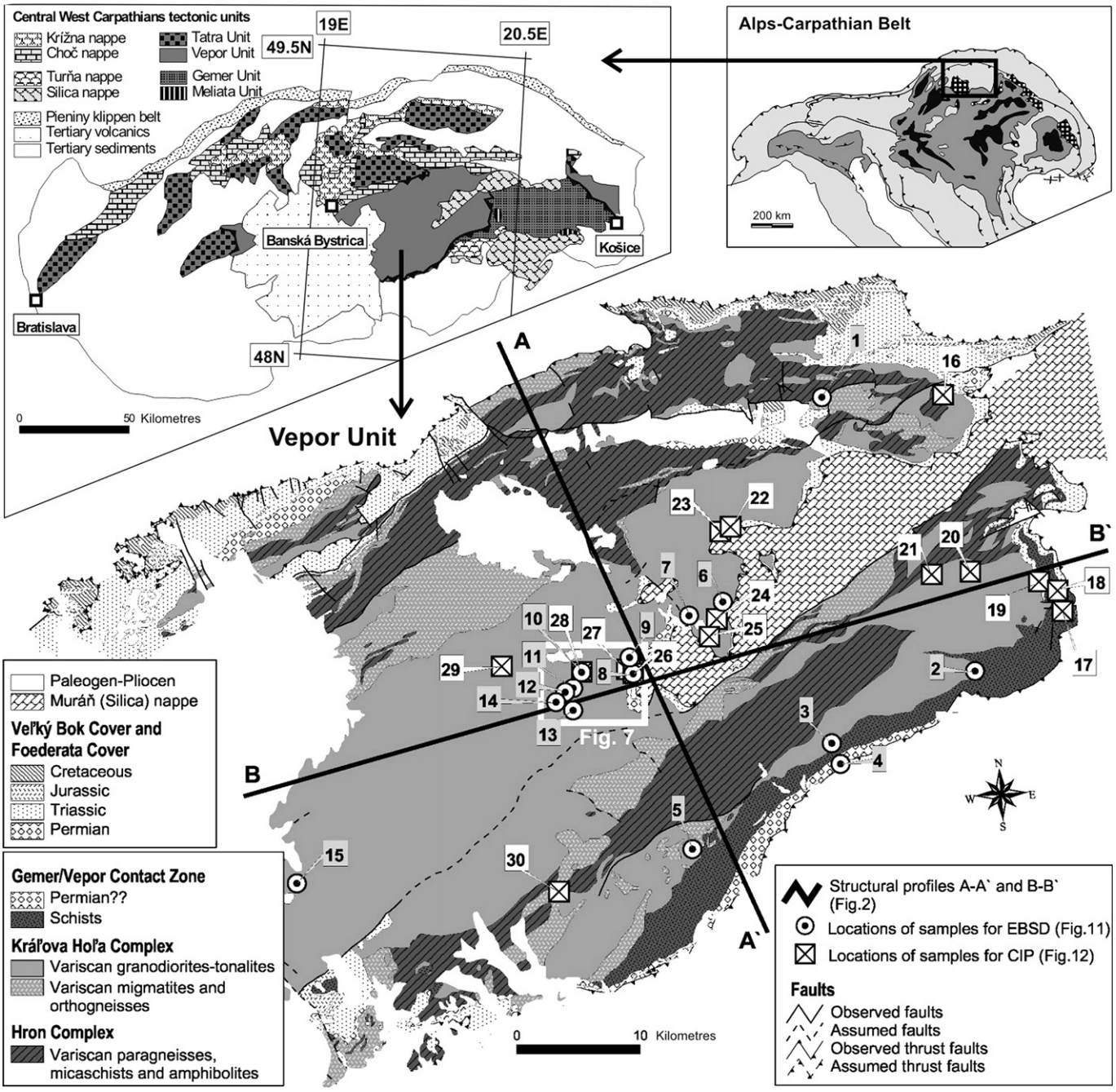

Fig. 1. Map of the Central West Carpathians region showing major tectonic units and the tectonic sketch of the Vepor Unit based on the collection of geological maps of ČSSR 1:200,000 (1963–1964). Vepor Unit is divided into four tectono-stratigraphic units: Foederata Cover and Vel'ký Bok Cover successions; Gemer/Vepor Contact Zone; Král'ova Hol'a Complex; Hron Complex. Locations of samples used for quartz texture analysis by Electron Back-Scattered Diffraction (EBSD) and by Computer Integrated Polarization microscopy (CIP) techniques are indicated in the figure as well as structural profiles A-A′ and B-B′ presented in Fig. 2. White rectangle corresponds to map section in Fig. 7.

In addition, the Late Variscan granitoids locally preserve a magmatic fabric characterized by shape preferred orientation of biotite and feldspars (cf. Siegl, 1982). The S_V fabric generally shows E–W trends in the areas unaffected by later deformation (Fig. 2).

The deformation event D_{A1} is characterized by the isoclinal folding and transposition of previous fabrics into a new penetrative metamorphic foliation S_{A1} in the Hron Complex, Král'ova Hol'a Complex and Gemer/Vepor Contact Zone, and isoclinal folding and transposition of bedding in the Foederata and Vel'ký Bok Cover (Figs. 2 and 3). In addition the late Variscan granitoids of the Král'ova Hol'a Complex show a heterogeneous development of solid state deformation fabric. With an exception of the Hron Complex, the deformation fabric S_{A1} gently dips to the East or South and it bears E–W to ENE–WSW trending stretching lineation L_{A1}, defined by alignment of feldspar and quartz and/or linear arrangement of micas. In some regions across the Vepor Unit the L_{A1} represents an

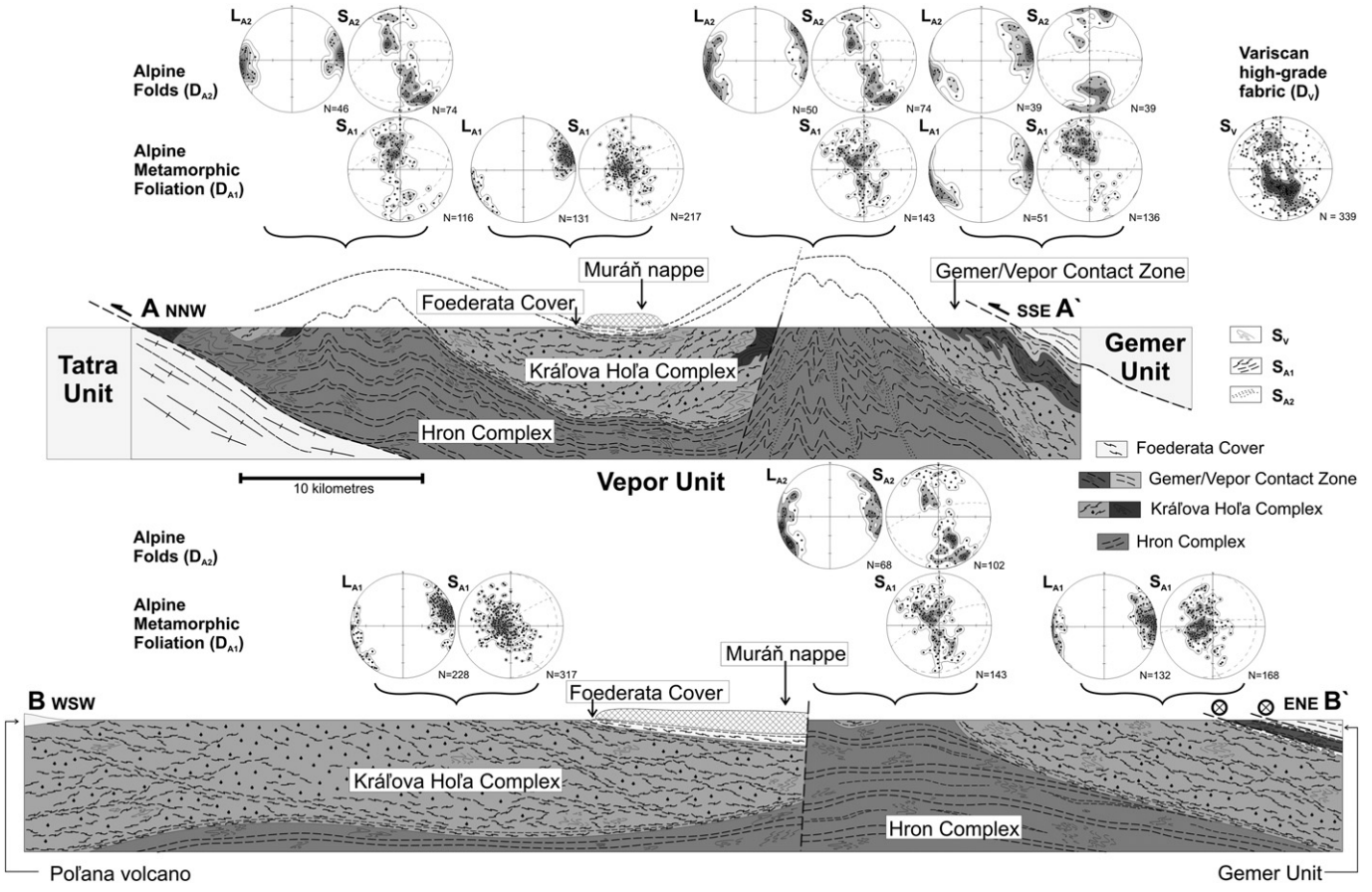

Fig. 2. NNW–SSE structural profile A-A′ and WSW–ENE structural profile B-B′ across the Vepor Unit shown in Fig. 1. Deformation structures are: S_V – Variscan metamorphic foliation, S_{A1} – Alpine metamorphic foliation, L_{A1} – Alpine lineation, S_{A2} – axial planes of F_{A2} – folds, L_{A2} – axis of F_{A2} folds, D_V – Variscan deformation event, D_{A1} – first Alpine deformation event, D_{A2} – second Alpine deformational event. The pole figures are lower hemisphere equal area Schmidt projections.

intersection lineation resulting from the superposition of the sub-horizontal S_{A1} over the older generally E–W trending S_V fabric. The intersection lineation is parallel to the axes of locally preserved isoclinal folds F_{A1}. In the Hron Complex, the S_{A1} fabric dips towards the NW or SE at shallow to steep angles (Figs. 2 and 3) mostly as a result of subsequent D_{A2} folding, which heterogeneously affects the entire Vepor Unit.

During the deformation event D_{A2}, large scale folds develop in the Hron Complex and Gemer/Vepor Contact Zone, while a crenulation cleavage affects the D_{A1} high strain domains in the Král'ova Hol'a Complex and in the cover formations. Generally, the F_{A2} folds have subvertical NE–SW to ENE–WSW trending axial planes and subhorizontal axis. In this study we concentrate on a detailed characterization of the first Alpine deformation event D_{A1}, which is best preserved in the deformed granitoids of the Král'ova Hol'a Complex (Fig. 4a) and overlying quartzite-arcose of the Foederata Cover (Fig. 4b).

3.1. Strain analysis

Strain analysis is based on the shape of recrystallized quartz aggregates (Fig. 5) and focuses on the record of D_{A1} within the granitoids of the Král'ova Hol'a Complex. The analysis was carried out at 59 sites using XZ sections (parallel to lineation and perpendicular to foliation) and YZ sections (perpendicular to lineation and foliation). Thin section photographs were taken in transmitted light with dark field illumination in order to distinguish darker quartz aggregates (Fig. 5). Aggregate outlines were digitized and processed in the PolyLX Matlab toolbox (Lexa, 2003). The number of digitized aggregates ranges from 20 to 100 with an average of 45 aggregates per sample. In order to estimate finite strain, the irregular shapes of individual quartz aggregates are approximated by ellipses representing the orientation tensor of decomposed boundaries (Scheidegger, 1965). The axial ratio (Rs) of the strain ellipse is calculated for both the XZ and YZ sections using the inverse strain modelling in PolyLX Matlab toolbox (arfphiw routine; Lexa, 2003). In this modelling the best Rs value is obtained by minimising the bulk weighted axial ratio according to:

$$W_{Rs} = \sum_{n=1}^{N} \left(R_n \frac{W_n}{\sum_{n=1}^{N} W_n} \right) \quad (1)$$

where R_n is axial ratio after the applied inverse strain Rs is parallel to the shape preferred orientation (SPO) and W_n is

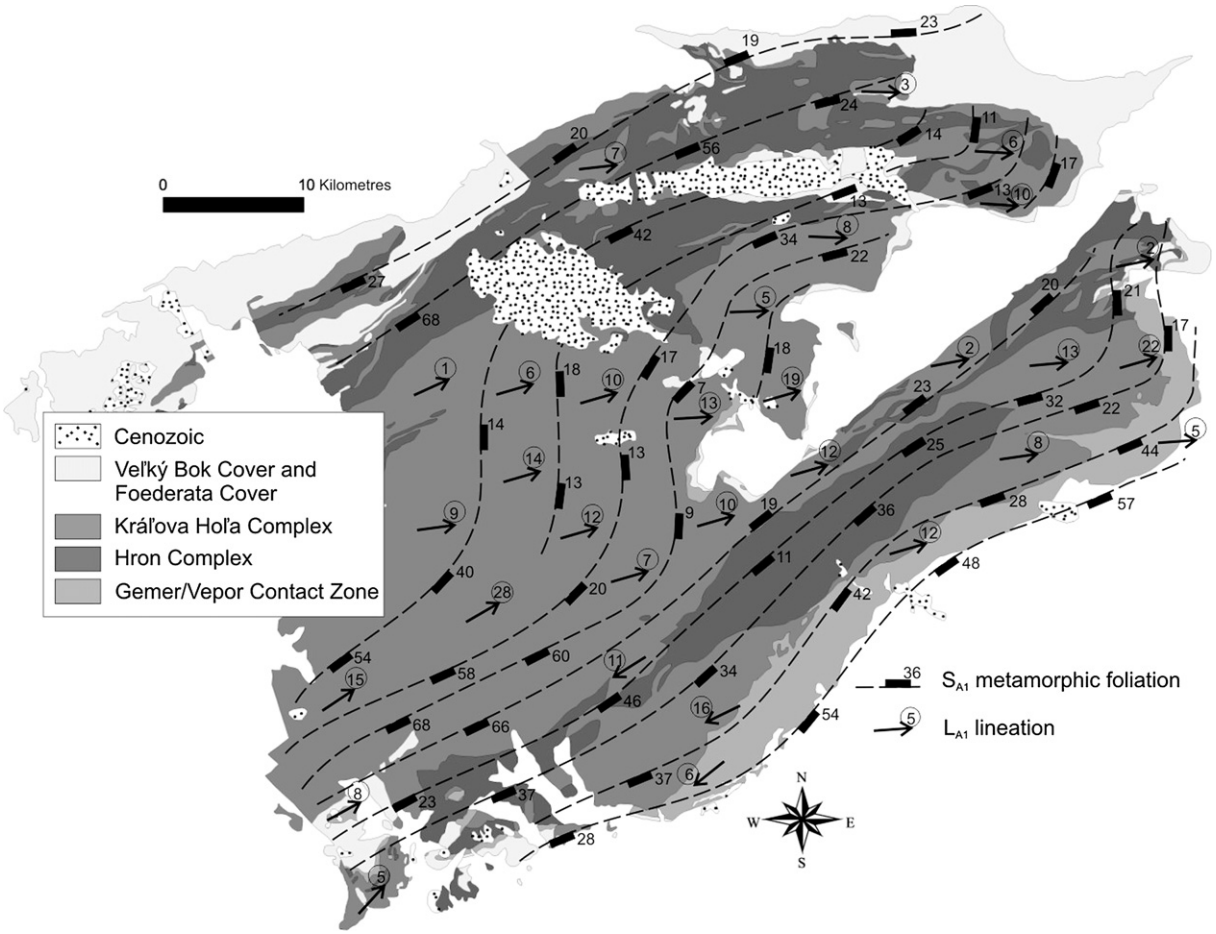

Fig. 3. Map of metamorphic foliation S_{A1} and lineation L_{A1} (average values are calculated using the Spheristat software).

the n-th aggregate weight, being linearly proportional to its area. Finally, the parameters of deformation symmetry (K) and deformation intensity (D) (Ramsay, 1967) are derived for each of the analysed sites.

The values of D of the quartz aggregates within granitoids of the Král'ova Hol'a Complex range between 0.34 and 1.7 and do not show substantial regional variations (Fig. 6a). The resulting D values, however, correspond to minimum strain estimates as the shapes of quartz aggregates underestimate the bulk strain because of deformation partitioning between the interconnected weak layers (matrix) and the stronger quartz aggregates. The values of K range between 0.05 and 6 and exhibit regional variations presented in Fig. 6b. Generally the finite strain ellipsoids of the central part of the Král'ova Hol'a Complex show

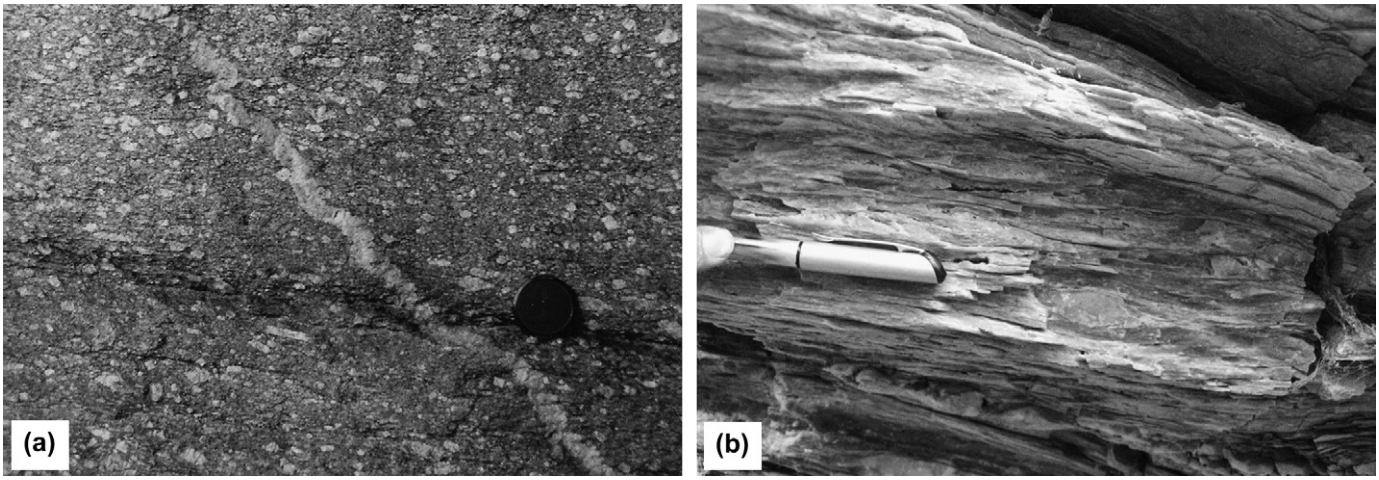

Fig. 4. (**a**) Deformed granitoids of the Král'ova Hol'a Complex. (**b**) Deformed quartzites of the Foederata Cover.

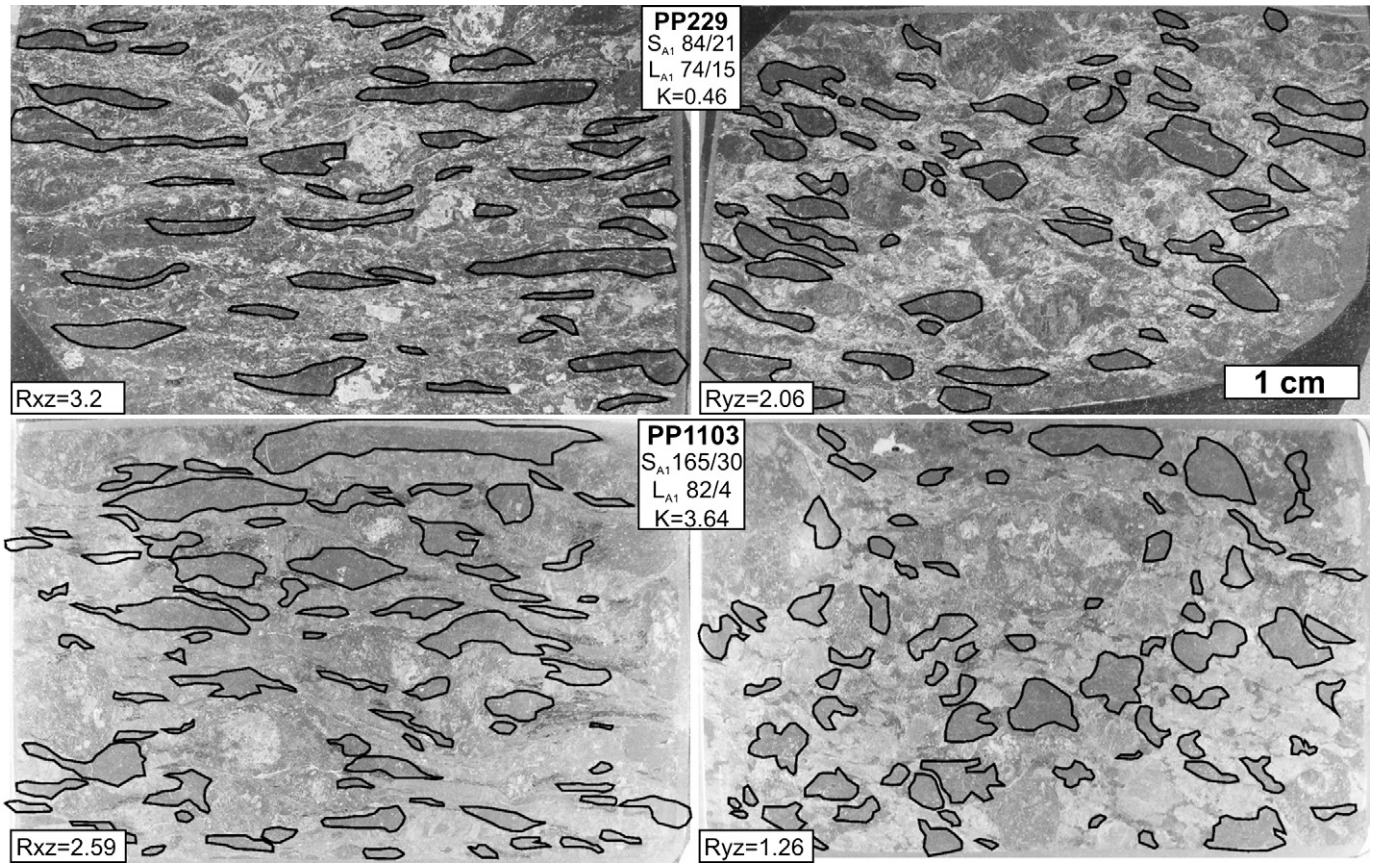

Fig. 5. Examples of oblate (PP229) and prolate (PP1103) type of finite strain (for location of samples see Fig. 6). Strain ellipsoids were determined using the shapes of recrystallized quartz aggregates in XZ and YZ thin sections. The strain ellipse ratios Rxz and Ryz as well as the resulting finite strain ellipsoid symmetry parameter (K) and the dip direction/dip of foliation (S_{A1}) and lineation (L_{A1}) for both the samples are indicated in the figure.

moderately oblate ($K < 1$) to plane strain symmetry that gradually passes to prolate symmetry ($K > 1$) towards the Northwest and Southeast of the Vepor Unit. The majority of the strain data in the Flinn diagram is concentrated below the plane strain ($K = 1$) line (Fig. 6). However, this is in part the effect of a smaller number of samples from the prolate regions of the Vepor basement where sampling is difficult due to a widespread occurrence of low strain and undeformed domains.

4. Microstructural record

The microstructural features of the granitoids do not vary much across the entire Král'ova Hol'a Complex. The microstructure is dominated by the first Alpine deformation event D_{A1}, although quartz also exhibits some relict microstructures of the pre-Alpine D_V and weak overprints of the second Alpine D_{A2} deformation. Texture analysis of plagioclase and quartz is used to infer the recrystallization mechanism, the type of strain and the kinematics of D_{A1}.

4.1. Changes of chemistry and composition – microstructural and metamorphic zonation

During D_{A1} the granitoids of the Král'ova Hol'a Complex experienced intense metamorphic and compositional changes (cf. Putiš et al., 1997). The magmatic mineral assemblage consisting of quartz, K-feldspar, oligoclase, muscovite, biotite and rarely allanite and garnet was replaced by the metamorphic mineral assemblage consisting of quartz, albite, phengitic muscovite, biotite, chlorite, epidote and calcium-rich garnet. The most important metamorphic transformations in terms of bulk microstructural changes in the granitoids are: (1) replacement of magmatic plagioclase by albite; (2) replacement of K-feldspar phenocrysts by polycrystalline albite and/or albite lamellae along the K-feldspar cleavage; and (3) formation of fine-grained muscovite (sericite) at the expense of feldspar. These reactions can be understood as a cation exchange between alkalis, where sodium released from the plagioclase is exchanged for potassium to form albite lamellae in the K-feldspar, while potassium from the K-feldspar is used to form sericite (Hippertt, 1998; and references therein). Calcium released from magmatic plagioclase is incorporated into epidote and grossular-rich garnet. In highly deformed granitoids, the modification of the bulk rock composition is often manifested by the formation of phyllonites of alternating sericite and quartz aggregates.

A detailed microstructural and petrographic study has been carried out on approximately 130 samples from 55 sites in the central part of the Král'ova Hol'a Complex (Fig. 7a). We identified an East–West metamorphic and microstructural zonation, indicating an increase in metamorphic P–T conditions

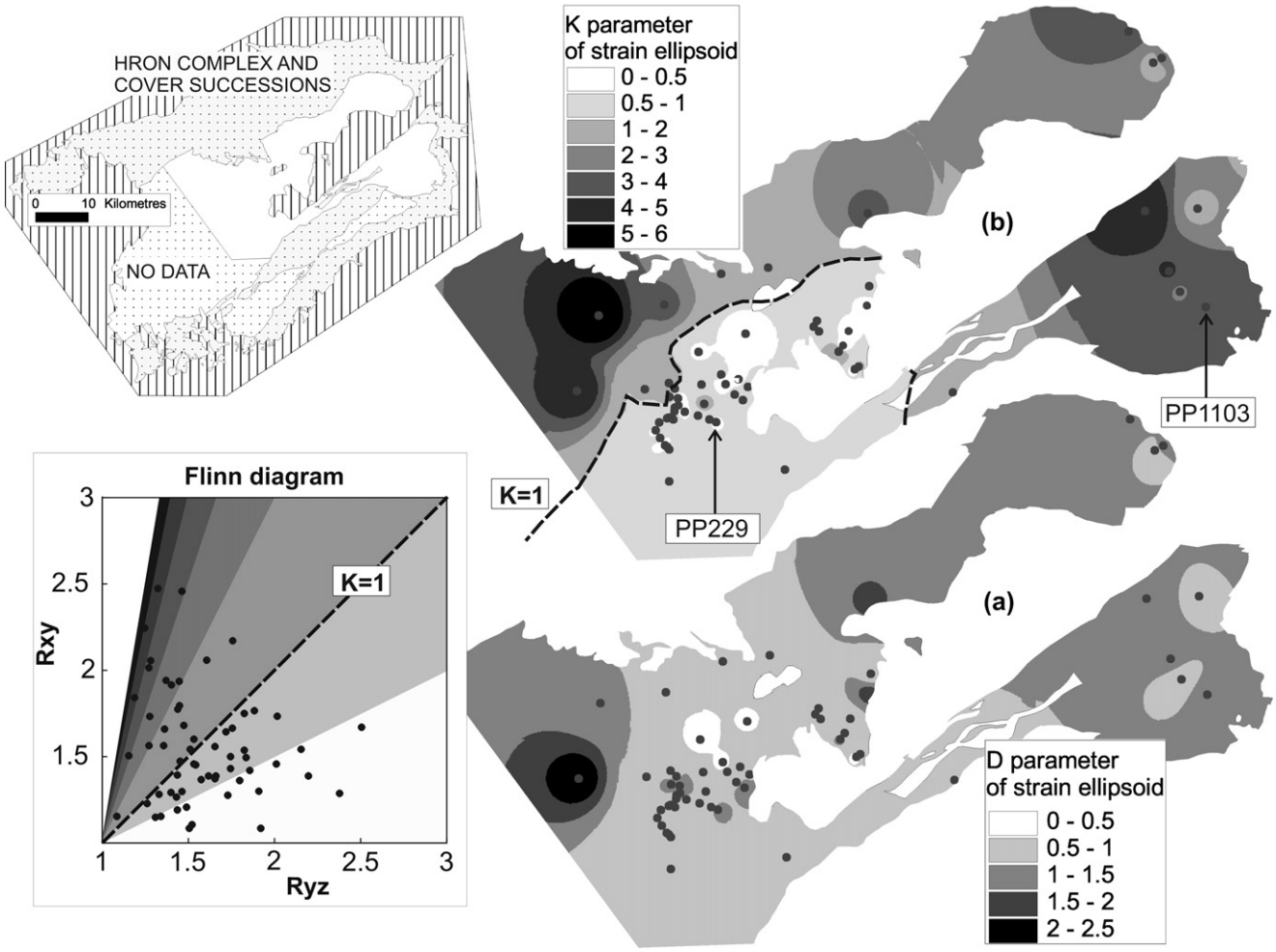

Fig. 6. The results of strain analysis presented in Flinn diagram and in the map of the Král'ova Hol'a Complex. The grid of deformation intensity parameter D (**a**); and deformation symmetry parameter K (**b**) were obtained by applying the inverse distance weighted (IDW) interpolation method in the MapInfo software. Dashed line K = 1 divides the Král'ova Hol'a Complex into two regions exhibiting dominantly prolate or oblate types of strain. Region of NO DATA corresponds to areas exhibiting minor overprint by the first Alpine deformation. Locations of samples PP229 and PP1103 (see Fig. 5) are indicated in (**b**).

towards the structural footwall in the West. The East to West metamorphic and microstructural changes comprise: (1) colour change of biotite from green to brown; (2) increasing modal proportion of biotite at the expense of chlorite; and (3) increasing grain size of the newly formed muscovite, biotite, plagioclase and recrystallized quartz. The bulk microstructural changes across the zonation were evaluated by using modal analysis (Fig. 7b). The analysis indicates Westward decrease in modal proportion of plagioclase and quartz porphyroclasts related to the progressive neocrystallization of albite and recrystallization of quartz. In contrast, the modal proportion of K-feldspar porphyroclasts increases, showing more intense replacement by muscovite in the East (Fig. 7b).

The modal analysis in the central part of the Král'ova Hol'a Complex was complemented with a petrological study. Using the phase equilibrium modelling in the software Perple_X (Connolly, 2005) and based on garnet isopleths, an increase in metamorphic conditions from 430–450 °C and 5.5 to 6.5 kbar in the East to 470–480 °C and 8–8.5 kbar in the West (Jeřábek et al., in press; Fig. 7c) can be inferred. The garnet compositional zoning records a prograde metamorphic evolution and an increase in P–T conditions of up to 25 °C and 1 kbar (Fig. 7c). The compositional zoning of garnets and prograde character of the Alpine metamorphism has also been recognised in other parts of the Vepor Unit (Méres and Hovorka, 1991; Kováčik et al., 1996; Plašienka et al., 1999; Janák et al., 2001; Jeřábek et al., in press).

4.2. Plagioclase microstructure

The plagioclase microstructure within granitoids of the Král'ova Hol'a Complex is largely controlled by metamorphic reactions (neocrystallization) during D_{A1}. Original magmatic plagioclase of unknown anorthite content and K-feldspar porphyroclasts are homogeneously replaced by albite (Fig. 8a), some disintegrate into albite and sericite matrix (Fig. 8b). Small neocrystallized albite grains (approx. 20 μm in the East of the central part of the Král'ova Hol'a Complex and 30 μm in the West) occur either in direct contact with the original porphyroclasts (preferentially in their pressure shadows) or dispersed in the matrix where they usually mix with quartz and sericite.

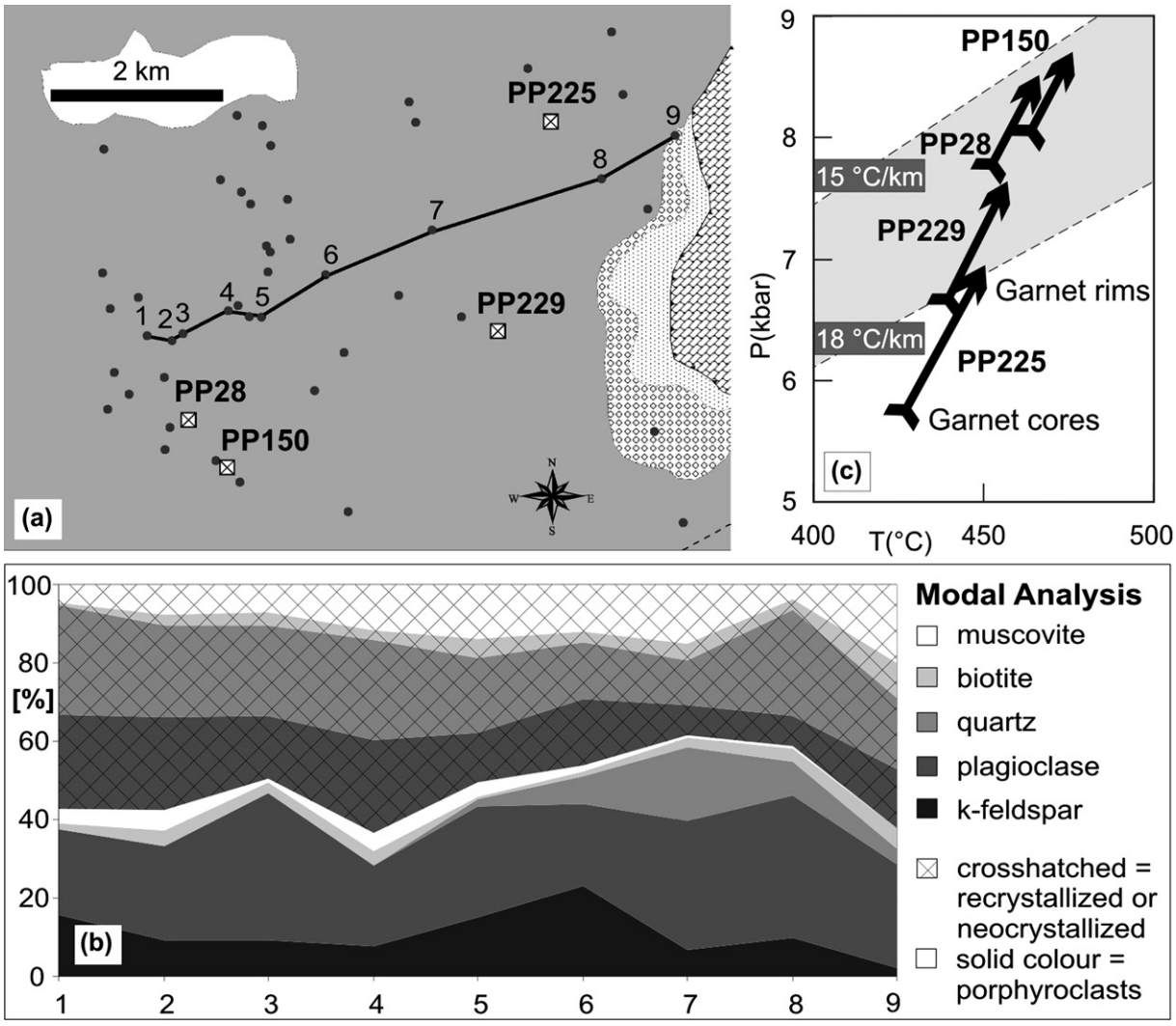

Fig. 7. (**a**) Map section corresponding to white rectangle in Fig. 1 showing sites of detailed microstructural analysis. (**b**) Modal analysis carried out from thin sections along the profile 1–9 illustrates the West to East bulk microstructural changes in the granitoids during D_{A1}. Crossed white squares in (**a**) indicate locations of samples (PP150, PP28, PP229 and PP225) used for P–T calculations in (**c**) (for details see Jeřábek et al., in press). (**c**) Arrows in the P–T diagram correspond to segments of prograde P–T paths determined for each of the four samples. Metamorphic gradient of 15 and 18 °C/km (dashed lines) is also indicated.

4.2.1. Plagioclase textures

Full crystallographic preferred orientation (CPO) of neocrystallized albite grains was measured on XZ thin sections using the electron back-scattered diffraction (EBSD) method. The EBSD patterns have been acquired using the HKL system attached to scanning electron microscope CAMSCAN 54 at the Institute of Petrology and Structural Geology, Prague. A total of 20 kV acceleration voltage, 39 mm working distance, ~5 nA beam current and 70° sample tilt were used.

The textures of albite single-phase matrix are characterized by weak (diagrams 10M and 14M in Fig. 9) or random CPO's (diagrams 1M, 12M and 13M in Fig. 9). In contrast, the pole figures of recrystallized albite grains in the immediate vicinity of plagioclase porphyroclasts show rather strong CPO's (diagrams 6 Cp, 7 Cp, 9 Cp, 11 Cp in Fig. 9) that coincide with the CPO of the original porphyroclasts (open squares in Fig. 9). This suggests a host controlled neocrystallization of albite induced by the metamorphic and compositional changes in the rock (Ji and Mainprice, 1988; Stünitz, 1998; Kruse et al., 2001). The absence of CPO in the highly deformed albite matrix and the weak CPO in less deformed albite matrix indicate a progressive destruction of the originally host controlled CPO's and a pervasive alignment of the CPO within the kinematic framework by diffusion creep deformation mechanism in the interconnected weak layers (Padmanabhan and Davies, 1980; Stünitz and Fitz Gerald, 1993; Rutter et al., 1994; Fliervoet et al., 1997; Newman et al., 1999).

4.3. Quartz microstructure

Granitoids of the Král'ova Hol'a Complex show three types of quartz deformation microstructures, characterized by different temperature conditions related to three main deformation events recorded in the Vepor Unit (Fig. 10). The microstructure, related to the first deformation, has only been observed in low strain domains preserved entirely from D_{A1}

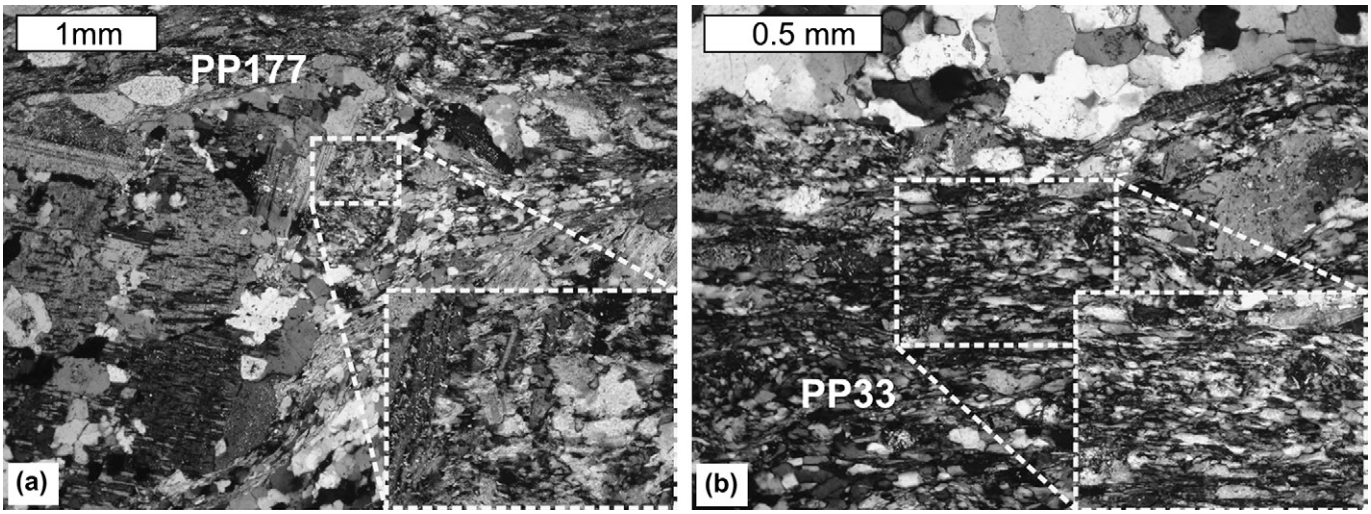

Fig. 8. Plagioclase microstructures: (**a**) replacement of K-feldspar porphyroclast by polycrystalline albite (left) and formation of small albite grains in the porphyroclast pressure shadow (centre), and (**b**) albite matrix. Rectangles highlight domains used for EBSD analysis; pole figures for the sample PP177 and PP33 are shown in Fig. 9 as 9Cp and 10M, respectively.

deformation. This microstructure is characterized by high temperature features such as island grains and lobate boundaries of large quartz grains (Fig. 10a), typical of high temperature grain boundary migration (GBM) as described by Stipp et al. (2002b). The earliest quartz microstructure probably coincides with the magmatic or high temperature stage of Late Variscan tectonic evolution.

The second deformation and the corresponding quartz microstructure are related to D_{A1} and can be found in the majority of analysed samples. It is characterized by the development of core and mantle microstructures in the East and centre of the Král'ova Hol'a Complex (Fig. 10b) and by completely recrystallized quartz aggregates, exhibiting lobate grain boundaries in the West (Fig. 10c). The presence of core and mantle microstructure indicates a dominance of rotation recrystallization (White, 1979) while the lobateness of grain boundaries suggests dominant strain induced grain boundary migration (Poirier and Guillope, 1979; Urai et al., 1986). Generally, the quartz microstructure across the whole Král'ova Hol'a Complex corresponds to the natural subgrain rotation recrystallization (SGR) microstructure of Stipp et al. (2002b). In the Easternmost parts of the Král'ova Hol'a Complex, the microstructures exhibit features characteristic for the transition from subgrain rotation to low temperature bulging recrystallization microstructures (SGR/BLG) (Fig. 10b), whereas in the central and Westernmost parts of the Král'ova Hol'a Complex they correspond to the transitional SGR/GBM (Stipp et al., 2002b) (Fig. 10c). Thus, there is a temperature or strain rate gradient (or both) from East to West. The deformation temperatures for the Easternmost parts of the Král'ova Hol'a Complex can be approximated by the metamorphic conditions of the overlying Foederata Cover indicating 380 °C (Lupták et al., 2003), while for the central and Westernmost parts of the Král'ova Hol'a Complex the metamorphic conditions of granitoids indicate 450–480 °C (Jeřábek et al., in press).

In the West, the previously-described quartz microstructures show a weak overprint by low temperature features such as small scale serration of grain boundaries and rare occurrence of small grains in the triple junctions of the larger quartz grains. This overprint can be correlated with the low temperature bulging recrystallization (BLG) of Stipp et al. (2002b). Similar overprint occurs also in the southeastern part of the Král'ova Hol'a Complex, where the low temperature recrystallization of quartz occurs along discrete shear surfaces crosscutting the deformation fabric S_{A1} (Fig. 10d). Thus, the low temperature overprints are associated with the folding during the second Alpine deformation D_{A2}, i.e., with a weak overprint of the Král'ova Hol'a Complex granitoids and intense folding of the Hron Complex paragneisses and micaschists.

4.3.1. Quartz textures

The CPO of recrystallized quartz grains has been determined from XZ thin sections either by using the electron back-scattered diffraction (EBSD) method or by using the computer integrated polarization (CIP) microscopy. The EBSD data acquisition is described in the ''Plagioclase microstructure'' section and the fundamentals of the CIP method are explained in Panozzo Heilbronner and Pauli (1993) and Heilbronner (2000).

The CPO of recrystallized quartz has been determined at 26 localities in the Král'ova Hol'a Complex and Foederata Cover (for locations of EBSD and CIP samples see Fig. 1) and the results are shown in Figs. 11 and 12. In order to compare the inclination of CPO's from all the analysed samples, the pole diagrams in Figs. 11 and 12 are presented within the same geographic reference frame, defined by the common orientation of generally East–West trending stretching lineation (see dip direction/dip of stretching lineation L_{A1} in Figs. 11 and 12). The most typical textures are single or crossed girdles, characterized by: (1) maxima located at or near the periphery of the c-axis pole figure and showing 20° half-aperture

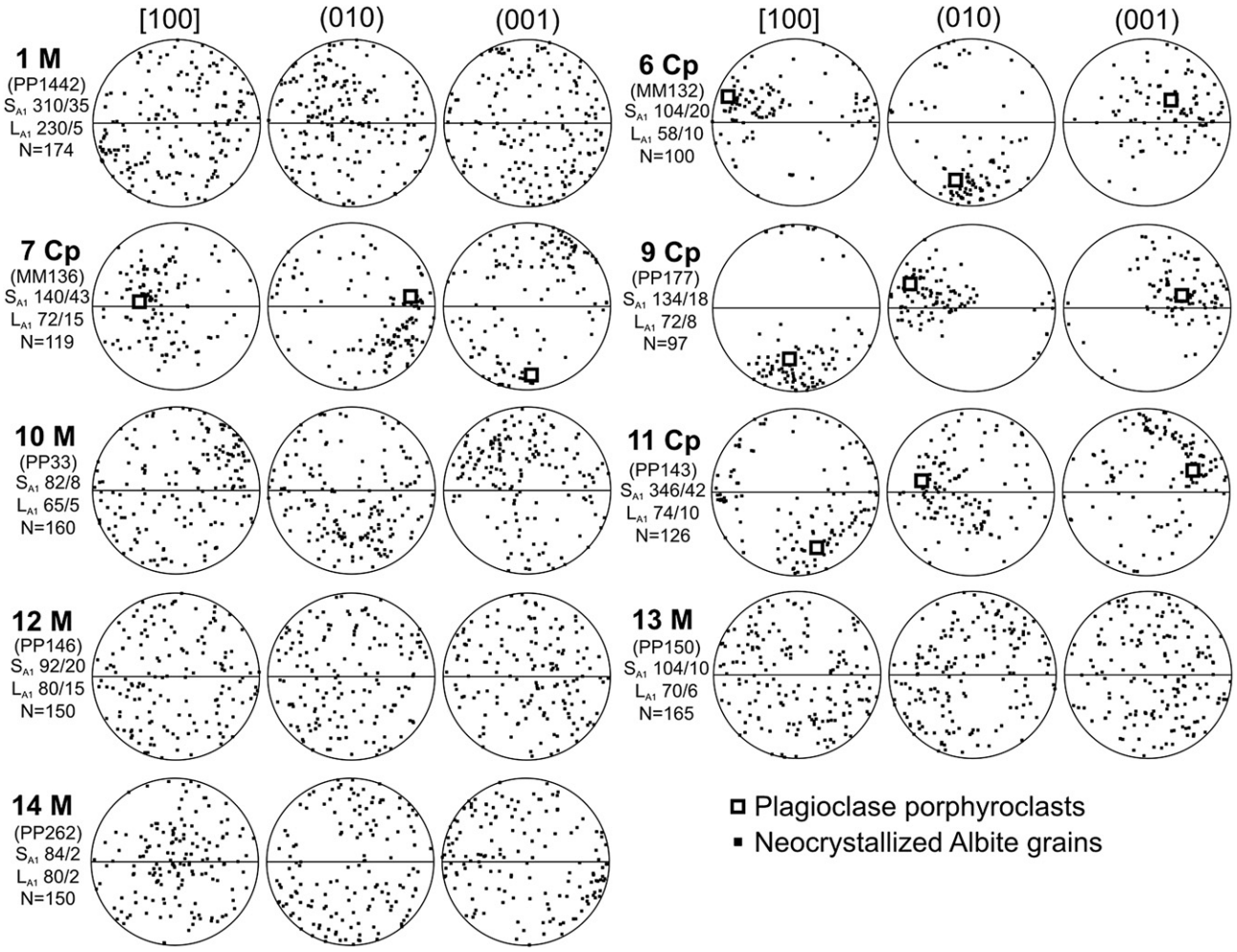

Fig. 9. Crystallographic orientation of recrystallized albite grains (small solid squares) obtained by Electron Back Scattered Diffraction (EBSD) in the XZ section of the finite strain ellipsoid. Lower hemisphere equal area projection pole figures represent [100] direction – [*a*-axis], poles to (010) plane and poles to (001) plane. Numbering of diagrams indicates sample locations in Fig. 1. Recrystallized grains (Cp) surrounding plagioclase porphyroclasts and recrystallized grains (*M*) in matrix are shown separately. *N* = number of measured grains. In the Cp diagrams open squares indicate orientation of the host grain. Original sample names and the dip direction/dip of foliation (S_{A1}, horizontal line in the pole figures) and stretching lineation (L_{A1}) are indicated in the figure.

(1Or, 5Qv, 7Or, 9Or in Fig. 11); and (2) by a single maximum near the centre of the c-axis pole figure (6Or, 9Or, 11Or, 14Or, 15Or in Fig. 11). Such patterns suggest that the deformation of quartz has taken place by dislocation creep on basal <*a*>, rhomb <*a* + *c*> and prism <*a*> slip systems (e.g. Schmid and Casey, 1986). The c-axis pole figures obtained by CIP (Fig. 12) show similar patterns as those obtained by EBSD (compare, e.g., diagrams 8Qu, 26Qv, 26Or and diagrams 10Or, 28Or in Figs. 11 and 12). Also there are no significant differences among the CPO's determined at the same location from different lithologies (compare, e.g., diagrams 26Or and 26Qv in Fig. 12).

The inclination of single or crossed girdle types of <*c*>-axis and <*a*>-axis pole figures with respect to foliation (Lister and Williams, 1979; Simpson and Schmid, 1983; Schmid and Casey, 1986) indicates either top-to-the-West (5Qv, 6Or, 9Or, 11Or, 14Or, 22Or, 26Or; Figs. 11 and 12) or top-to-the-East (21Or, 24Or; Figs. 11 and 12) sense of movement, or yield no conclusive shear senses. However, the texture analysis clearly demonstrates that conflicting shear senses occur even within the same thin section as exemplified in Fig. 13. This observation is consistent with other microscopic shear sense indicators (e.g. sigma porphyroclasts, book shelves), which mostly do not exhibit an unequivocal sense of shearing within a single thin section. Our regional shear sense determinations contrast with the overall top-to-the-East sense of shearing, reported, e.g., by Putiš et al. (1997), Plašienka et al. (1999) and Hrouda et al. (2002).

5. Estimates of differential stress and strain rate

In this section we concentrate on the determination of differential stresses and strain rates within granitoids of the Král'ova Hol'a Complex during the D_{A1}. The recrystallized quartz grain size is evaluated as a function of the microstructural zonation at the BLG/SGR transition (Stipp et al., 2002b) at 380 °C (Lupták et al., 2003) in the Easternmost parts of the Král'ova Hol'a Complex and at the SGR/GBM transition at

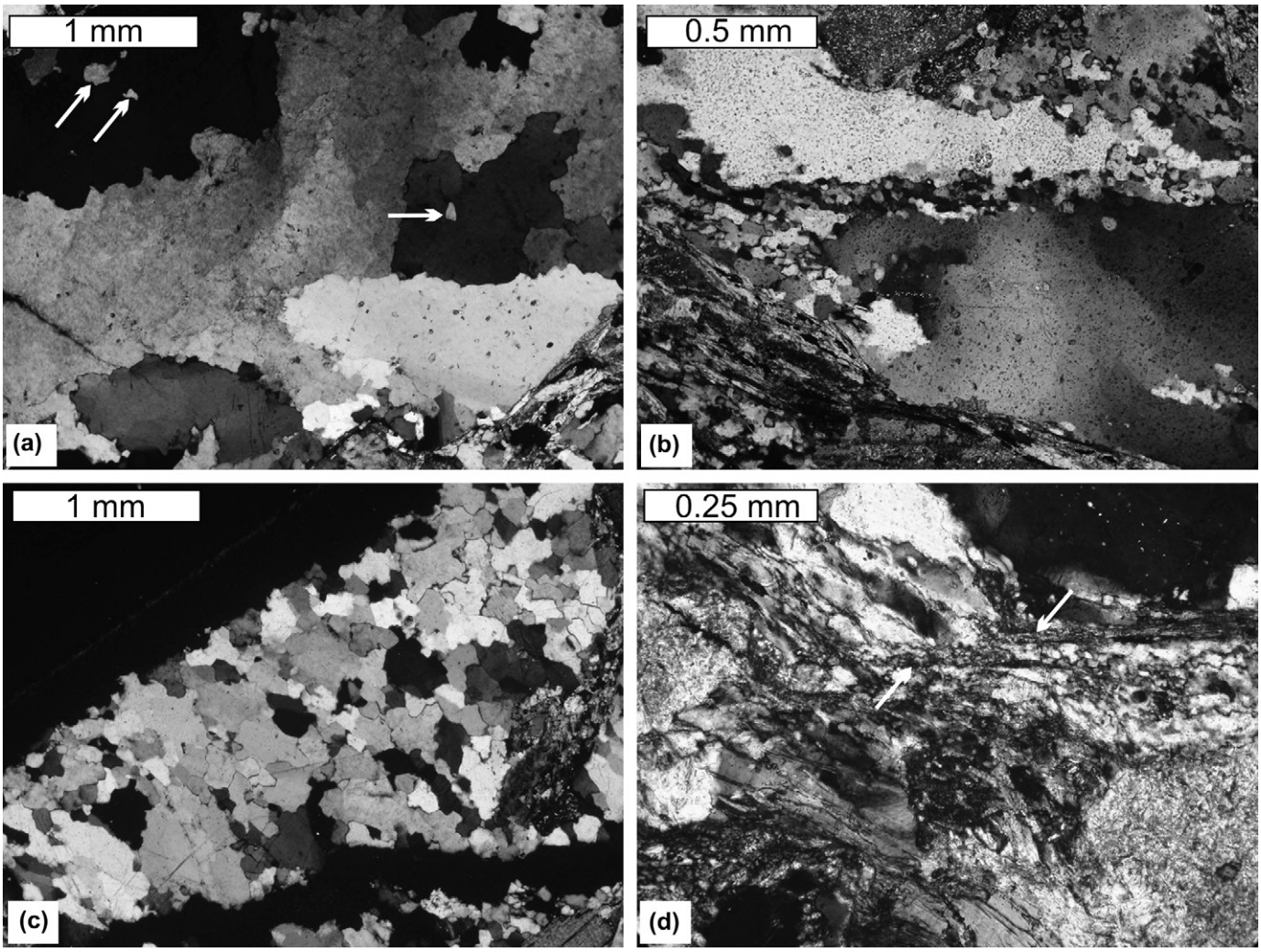

Fig. 10. Three varieties of quartz deformation microstructures in the granitoids of the Král'ova Hol'a Complex. (**a**) island grains (arrows) and lobate grain boundaries at high temperatures (see text); (**b**) core and mantle microstructure and transition between SGR/BLG microstructure at medium temperatures; (**c**) lobate grain boundaries and transition between SGR/GBM microstructure at medium temperatures; and (**d**) recrystallization along discrete shear surfaces (arrows) at low temperatures.

480 °C (Jeřábek et al., in press) in the central and Westernmost parts of the Král'ova Hol'a Complex.

5.1. Recrystallized quartz grain size

Recrystallized quartz grain sizes have been determined from XZ thin sections at 102 sites, distributed over the entire Král'ova Hol'a Complex. An interpolated map of recrystallized grain size is shown in Fig. 14. Fully recrystallized quartz aggregates (Fig. 10c) and recrystallized grains in the vicinity of original quartz porphyroclasts (Fig. 10b) have been selected for the analysis. The absence of interfering second phase particles inside the recrystallized quartz aggregates has been verified by light microscopy at high magnifications. Local variations in the recrystallized quartz grain size, related to stress concentrations in the vicinity of strong plagioclase and K-feldspar porphyroclasts (Handy, 1990; Prior et al., 1990), are avoided by analysing the aggregates with intermediate grain size. We have used the automatic grain boundary detection method of Heilbronner (2000) and – for each analysis – a set of nine cross-polarized photomicrographs, obtained by rotating both the polarizer and analyzer within an interval of 0–90°. The diameter of each grain (defined as diameter of a circle with the same area) has been calculated from digitized grain boundary maps using the PolyLX Matlab toolbox (Lexa, 2003). The number of measured grains range from 250 to 1000 with the average of 520 grains per sample. Due to the log-normal nature of analyzed grain diameter distributions, the median has been used to characterize the average recrystallized quartz grain size in each sample (Ranalli, 1984) and an interquartile range (IQR) defined as the difference between upper and lower quartile of the grain size distribution has been used to determine the confidence interval.

The recrystallized quartz grain size shows systematic variations across the Král'ova Hol'a Complex along the ENE–WSW as well as NNW–SSE gradient (Fig. 14). On the interpolated grain size map the contour lines are subparallel to the trendlines of the deformation fabric S_{A1} (Fig. 3) indicating that the

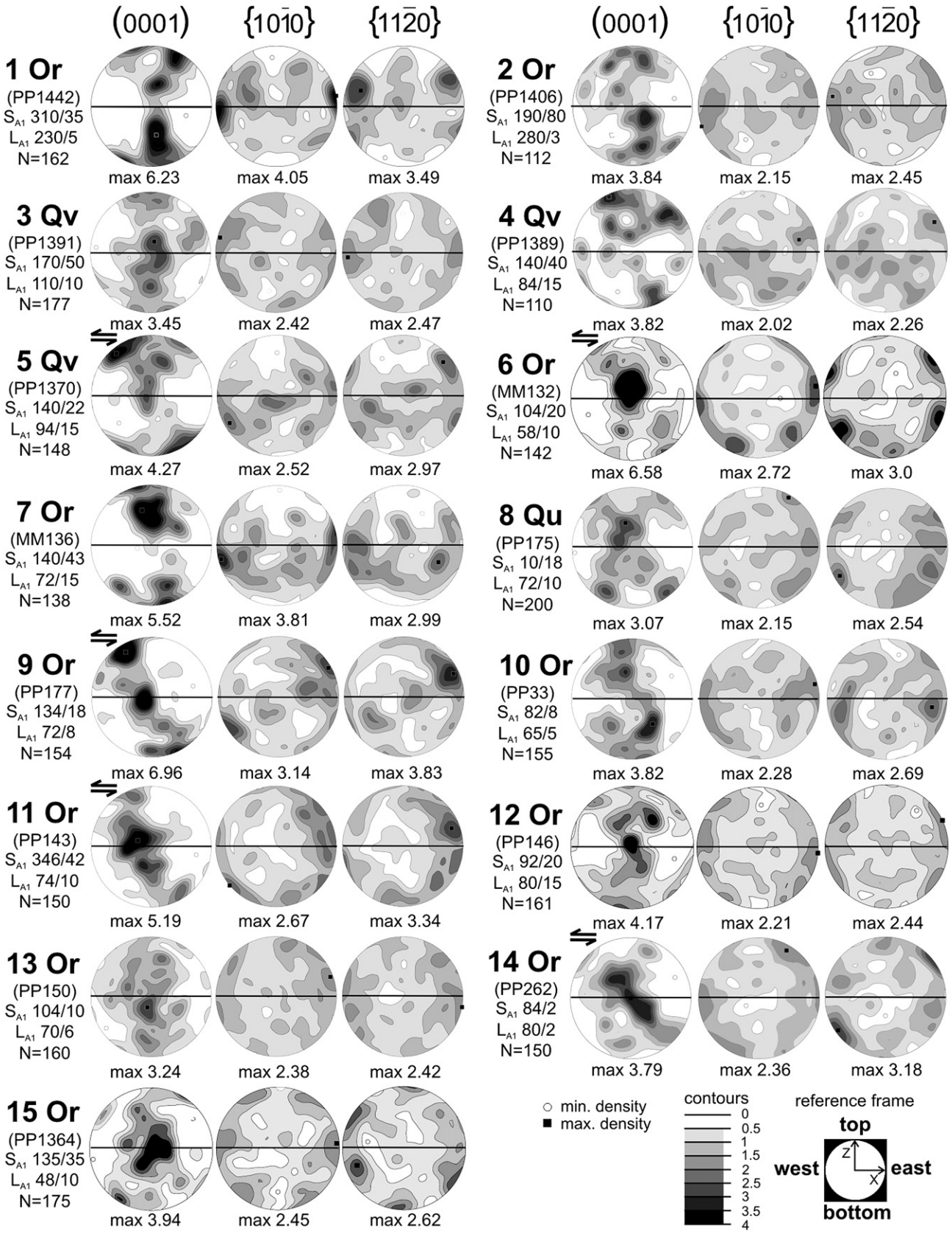

Fig. 11. Crystallographic orientation of recrystallized quartz grains measured by Electron Back Scattered Diffraction (EBSD) in the XZ section of the finite strain ellipsoid. Lower hemisphere equal area projection pole figures represent poles to base (0001) [*c*-axis], poles to the first order prism {10−10} <*m*-axes> and poles to the second order prism {11−20} <*a*-axes>. Numbering of diagrams indicates sample locations in Fig. 1. Or − orthogneiss samples, Qv − quartz veins samples, Qu − quartzite samples. Original sample names, the dip direction/dip of foliation (S_{A1}, horizontal line in the pole figures) and stretching lineation (L_{A1}), and the number of measured grains (N) are also indicated. Contours refer to multiples of the uniform density distribution; the geographic reference frame common to all presented pole figures is shown in lower right. The arrows indicating sense of shear are determined from inclination of single and crossed girdles with respect to the foliation S_{A1}.

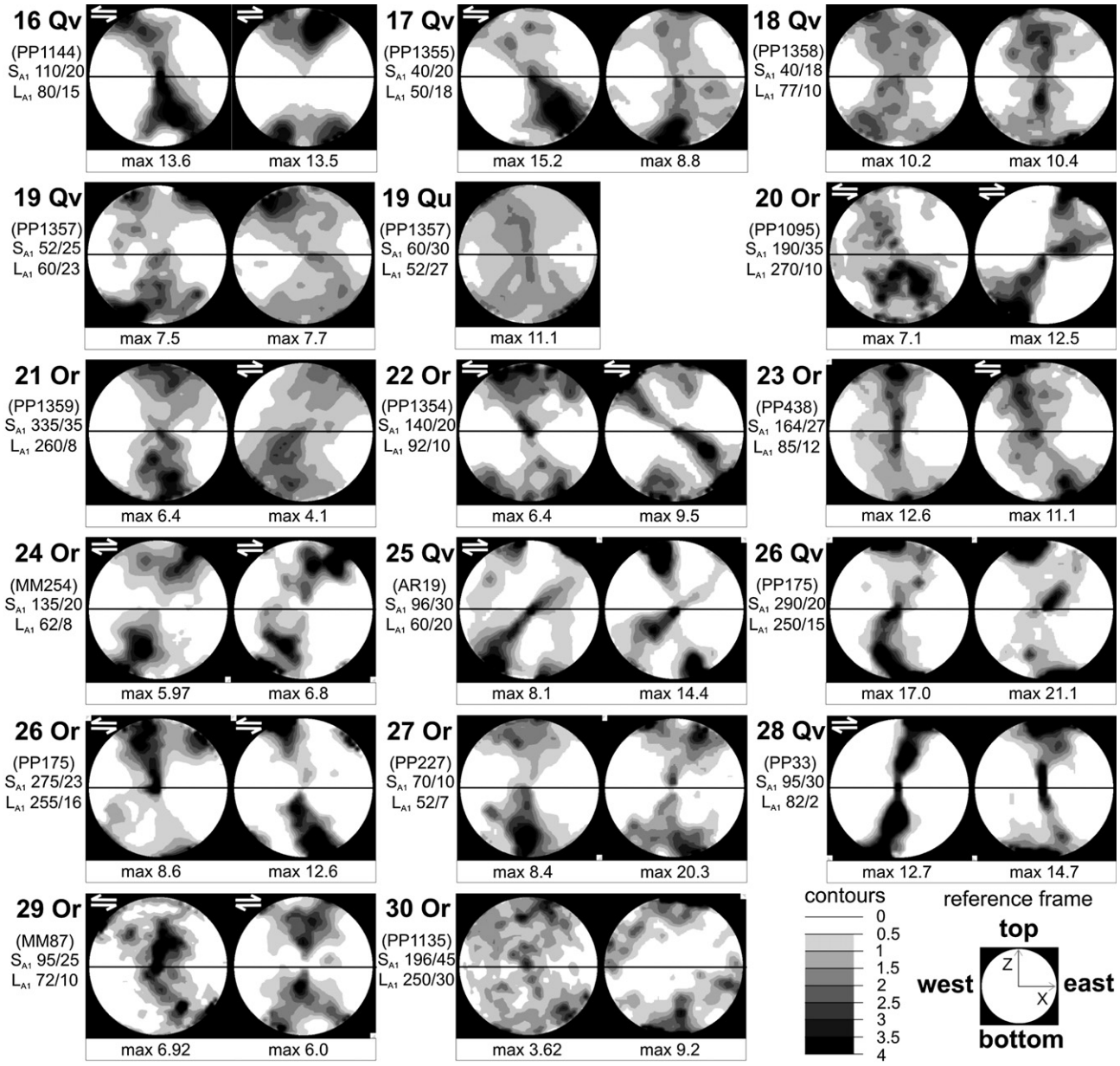

Fig. 12. *C*-axis pole figures of recrystallized quartz grains obtained by using Computer Integrated Polarization (CIP) microscopy technique in the XZ section of the finite strain ellipsoid. Numbering of diagrams indicates sample locations in Fig. 1. Or – orthogneiss samples, Qv – quartz veins samples, Qu – quartzite samples. Two pole figures for each location were obtained by analysing different areas within one thin section. Original sample names and the dip direction/dip of foliation (S_{A1}, horizontal line in the pole figures) and stretching lineation (L_{A1}) are also indicated. Contours refer to multiples of the uniform density distribution; the geographic reference frame common to all presented pole figures is shown in lower right. The arrows indicating sense of shear are determined from inclination of single and crossed girdles with respect to the foliation S_{A1}.

recrystallized grain size decreases towards the structural hanging wall Foederata Cover, occurring in the East and centre of the Vepor Unit (compare Figs. 1 and 14). In the vicinity of the Foederata Cover in the East the median grain size reaches a minimum of 28 μm; a maximum of 100 μm is found in the West (Fig. 14). The interquartile range (IQR) is 63 μm on average with a minimum and maximum value of 19 and 89 microns, respectively. The grain size increase towards the structural footwall is paralleled by an increase in temperature in the central part of the Král'ova Hol'a Complex. Here the westward increase in peak P–T conditions (Fig. 7) from 450 °C and 6.5 kbar to 480 °C and 8.5 kbar (Jeřábek et al., in press) corresponds to an increase in median recrystallized quartz grain size from 70 to 83 microns (Fig. 14).

5.2. Differential stress estimates from recrystallized quartz

Among the experimentally calibrated piezometers (Mercier et al., 1977; Christie et al., 1980; Koch, 1983; Stipp and Tullis, 2003), the most recent piezometer of Stipp and Tullis (2003), established for the experimental dislocation creep regimes

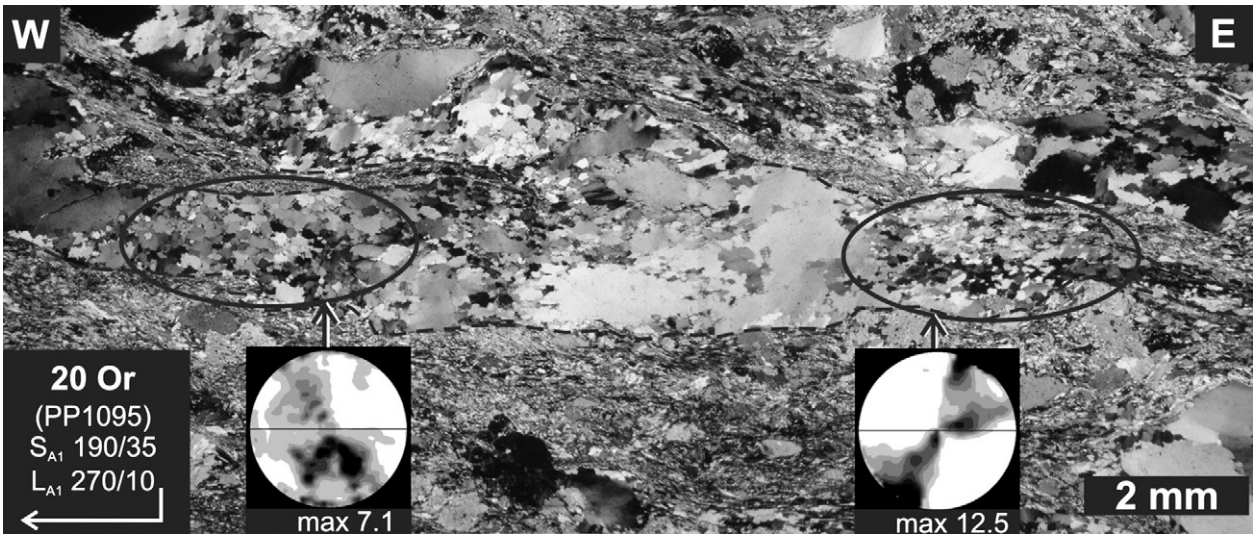

Fig. 13. The XZ section of the sample PP1095 shows recrystallized quartz aggregate with core and mantle microstructure. The corresponding CIP *c*-axis pole figures (diagrams number 20 in Fig. 12) of recrystallized quartz within selected regions (ellipses) are shown. E–W directions and the dip orientation of foliation (S_{A1}) and lineation (L_{A1}) are also indicated.

2–3 (Hirth and Tullis, 1992), provides the best mechanical constraints in terms of stress resolution, steady state control and starting material for wet quartz. At the same time, the theoretical piezometer of Twiss (1977) has been used in most of the recent studies on natural mylonites (Dunlap et al., 1997; Stöckhert et al., 1999; Stipp et al., 2002a) following the recommendation of Gleason and Tullis (1993, 1995). We have therefore used both piezometers to constrain differential

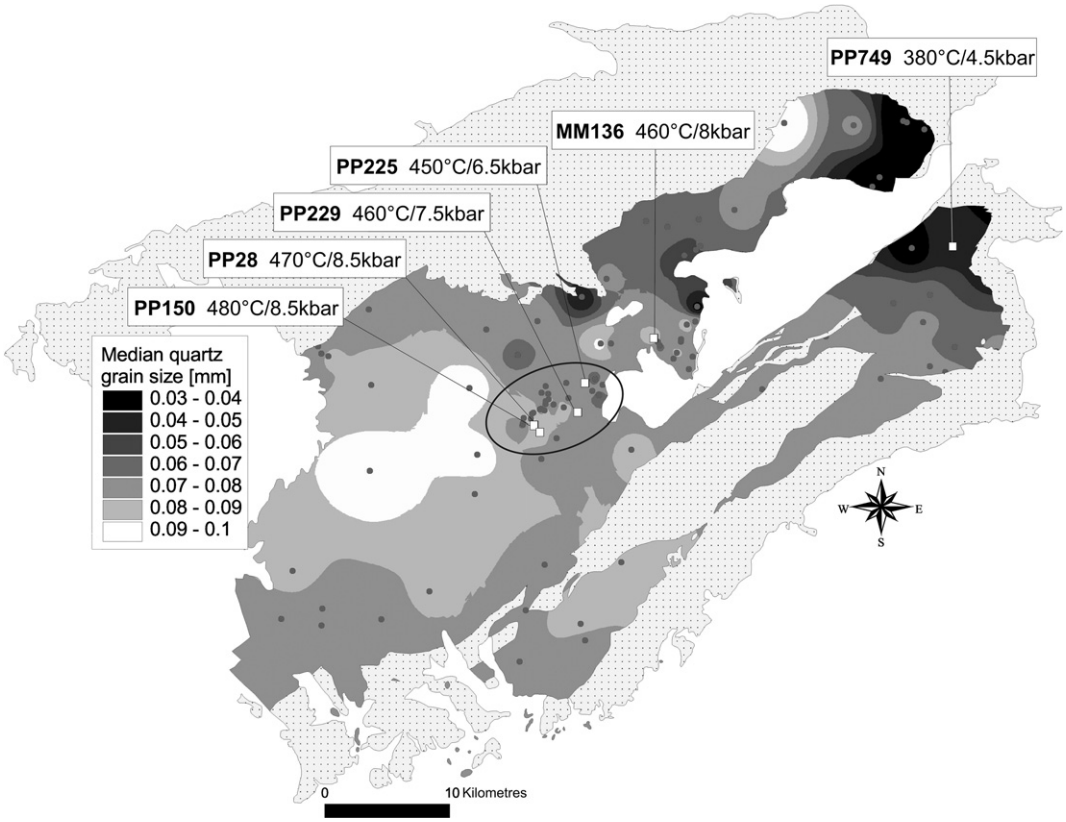

Fig. 14. Measured + interpolated grain size of recrystallized quartz across the Král'ova Hol'a Complex. Medians of the grain size distribution determined from indicated sites served as input for the grid calculation by the inverse distance weighted (IDW) interpolation method in the MapInfo. White squares indicate locations of samples used for strain rate estimates (see text and Table 2). P–T conditions for samples PP150, PP28, PP229, PP225 and MM136 were taken from Jeřábek et al. (in press). For sample PP749, we used the P–T estimates from nearby sample DOPO2 of Lupták et al. (2003). Ellipse shows a locus of a detailed microstructural analysis (see Fig. 7 and text for explanation).

stresses within the Král'ova Hol'a Complex. The piezometers are applied in the form:

$$\Delta\sigma = BD^{-p} \quad (2)$$

where $\Delta\sigma$ is the differential stress, D is the recrystallized grain size, and B and p are empirical constants ($B = 677.42$ and $p = 0.68$ for Twiss, 1977; $B = 668.95$ and $p = 0.7936$ for Stipp and Tullis, 2003).

The investigated quartz microstructures do not indicate annealing, so that grain growth (Hacker et al., 1990, 1992) or other modification (Heilbronner and Tullis, 2002) did not have to be considered. The median recrystallized quartz grain size ranges between 28 and 100 μm in the Král'ova Hol'a Complex and indicates differential stresses for recrystallized quartz between 17 and 47 MPa (using the piezometer of Stipp and Tullis, 2003), and between 29 and 69 MPa (using the piezometer of Twiss, 1977).

5.3. Strain rate

The strain rate in natural conditions can be calculated by using experimentally derived flow laws extrapolated to natural conditions. The suggestion of Paterson (1989) to include the water fugacity term into the flow law has been followed by Gleason and Tullis (1995), Kohlstedt et al. (1995) and Post et al. (1996) and their flow law takes the following form:

$$\dot{\varepsilon} = A\Delta\sigma^n f_{(\mathrm{H2O})}^m \exp(-Q/\mathrm{RT}) \quad (3)$$

where $\dot{\varepsilon}$ is the strain rate, A is a material constant, $\Delta\sigma$ is the differential stress, n is the stress exponent, $f_{(\mathrm{H2O})}$ is the water fugacity, m is the water fugacity exponent, Q is the creep activation energy per mole, R is the Boltzmann constant per mole and T is the temperature.

The coefficients A, n and Q for the experimentally determined flow law by Luan and Paterson (1992) as well as the geologically constrained empirical flow laws of Paterson and Luan (1990) and Hirth et al. (2001) (Fig. 15) are listed in Table 1. The water fugacity exponent is set to $m = 1$ following Kohlstedt et al. (1995) and Hirth et al. (2001). In order to reduce the differences in water fugacity and to adjust the flow laws to the deformation conditions of the Král'ova Hol'a Complex granitoids, the flow law curves in Fig. 15 are normalised to water fugacities corresponding to the confining pressures obtained from the average Alpine metamorphic field gradient of 16.5 °C/km (Jeřábek et al., in press) and the average rock density of 2700 kg/m^3. The fugacity coefficients of Tödheide (1972) were used.

Differential stress, temperature and pressure determined at six sites reflecting different vertical levels of the Král'ova Hol'a Complex (see Fig. 14) have been used to calculate the strain rate during D_{A1} (Table 2). Peak P–T estimates for the samples PP28, PP150, PP225, PP229 and MM136 (central part of the Král'ova Hol'a Complex; Figs. 7 and 14) have been taken from Jeřábek et al. (in press). For the sample

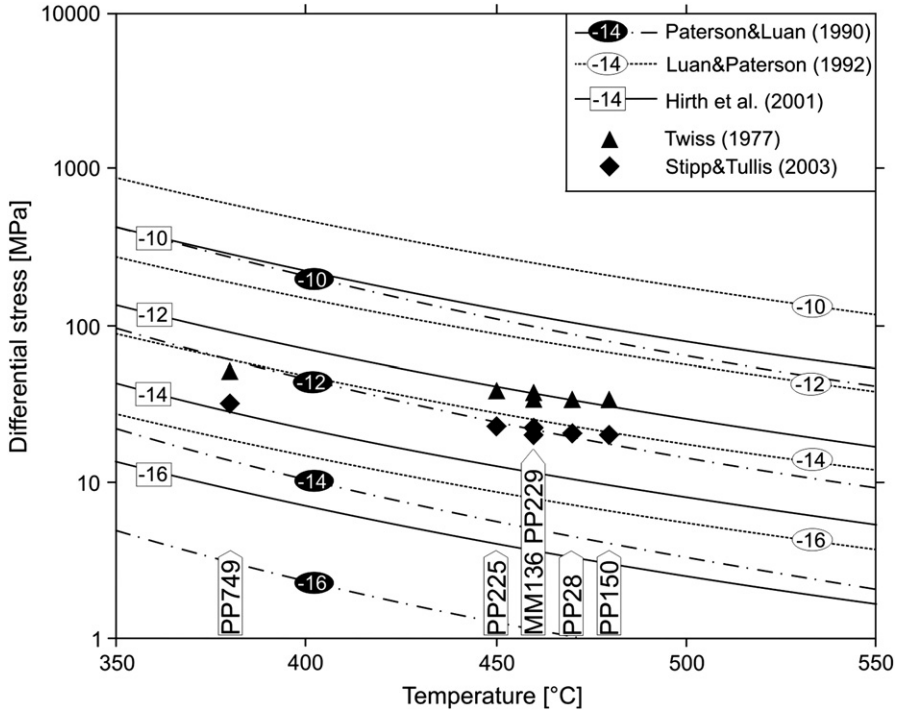

Fig. 15. Differential stress and temperature diagram showing differential stresses and temperatures determined at six sites within the Král'ova Hol'a Complex (for locations see Fig. 14 and for stress and temperature data see Table 2). Triangles indicate differential stresses obtained according to the piezometer of Twiss (1977) and diamonds those according to Stipp and Tullis (2003). Curves of constant strain rate are calculated from flow laws of Paterson and Luan (1990), Luan and Paterson (1992) and Hirth et al. (2001). All the flow laws are normalized to water fugacities at temperatures and confining pressures using the average Alpine metamorphic field gradient of 16.5 °C/km (Jeřábek et al., in press).

Table 1
Coefficients of the flow laws used in this study

	Q [kJ mol^{-1}]	A [MPa^{-n} s^{-1}]	N
Paterson and Luan (1990)	135	6.5×10^{-8}	3.1
Luan and Paterson (1992)	152	4×10^{-10}	4
Hirth et al. (2001)	135	6.30957×10^{-12}	4

PP749 (Easternmost part of the Král'ova Hol'a Complex; Fig. 14), the peak P–T estimate from nearby Foederata Cover (sample DOPO2 of Lupták et al., 2003) was used. The flow laws of Paterson and Luan (1990), Luan and Paterson (1992) and Hirth et al. (2001) were used because they also match the wide range of the conditions at the Eastern Tonale mylonite zone (see Fig. 7 in Stipp et al., 2002a). Using the differential stresses obtained by the piezometer of Stipp and Tullis (2003) and Twiss (1977), the strain rates determined by the three flow laws are in the range of 10^{-12}–10^{-16} s^{-1} and 10^{-11}–10^{-15} s^{-1}, respectively (Table 2, Fig. 15).

6. Discussion

6.1. Stretching of the Vepor Unit perpendicular to orogenic shortening

The orientation of the lineation defined by shape preferred orientation of quartz aggregates and micas in conjunction with the quartz texture analysis indicate that during the development of the subhorizontal deformation fabric S_{A1}, the Vepor Unit underwent stretching in the East–West direction, i.e., parallel to the strike of the Cretaceous West Carpathian orogen.

The shape analysis of deformed quartz aggregates shows predominantly plane strain to moderately oblate ellipsoids in the highly deformed central area of the Král'ova Hol'a Complex and plane strain to prolate ellipsoids towards its marginal parts (Fig. 6). This observation contrasts with the shape of skeletons of the quartz c-axis pole figures, which despite the heterogeneity of quartz CPO's related to low strain of the quartz aggregates ($D = 0.34$–1.7), suggests an overall plane strain symmetry (Schmid and Casey, 1986) of the first Alpine deformation D_{A1} (Figs. 11 and 12). This discrepancy can be explained by the different capacity of SPO and CPO to record the deformation history. The subhorizontal and dominantly plane strain deformation fabric S_{A1} has been superposed on the pre-existing Variscan fabric S_V, which generally exhibits East–West trends in the areas unaffected by the Alpine deformation. Consequently, the prolate shapes of quartz aggregates may occur in areas with an originally steeply dipping pre-Alpine fabric whereas the oblate aggregates may occur in areas with an originally gently-dipping pre-Alpine fabric. Thus while the SPO records the cumulative effect of D_V and D_{A1}, the quartz CPO is completely reset by D_{A1}.

In many instances the asymmetrical character of the CPO suggests plane strain simple shear. However, the inclination of the c-axis with respect to the foliation S_{A1} as well as other microscopic shear sense indicators do not show a consistent sense of shear across the Vepor Unit. Therefore the

Table 2
Recrystallized quartz grain size with upper and lower quartile as the confidence interval (±values), and temperature and pressure estimates (PP28, PP150, PP225, PP229 and MM136 from Jeřábek et al. (in press), and PP749/DOPO2 from Lupták et al. (2003), see text for explanation) determined at six sites within the Král'ova Hol'a Complex (for locations see Fig. 14)

Samples	Number of measured grains	Median grain size [μm]	Inter-quartile range (IQR) [μm]	Tem-perature [°C]	Lithostatic pressure [MPa]	Fugacity coefficients of water Tödheide (1972)	Fugacity of water [MPa]	Differ-ential stress [MPa] Stipp and Tullis (2003)	Strain rate [s^{-1}] Paterson and Luan (1990)	Strain rate [s^{-1}] Luan and Paterson (1992)	Strain rate [s^{-1}] Hirth et al. (2001)	Differ-ential stress [MPa] Twiss (1977)	Strain rate [s^{-1}] Luan and Paterson (1992)	Strain rate [s^{-1}] Luan and Paterson (1992)	Strain rate [s^{-1}] Hirth et al. (2001)
PP150	320	83^{+48}_{-30}	78	480	850	0.6638	564.23	20	1.78×10^{-12}	1.08×10^{-14}	2.48×10^{-13}	34	8.77×10^{-12}	8.42×10^{-14}	1.94×10^{-12}
PP28	335	82^{+55}_{-24}	79	470	850	0.6382	542.47	20	1.38×10^{-12}	8.17×10^{-15}	1.86×10^{-13}	34	6.79×10^{-12}	6.34×10^{-14}	1.44×10^{-12}
MM136	431	83^{+59}_{-29}	88	460	800	0.558	446.4	20	8.67×10^{-13}	4.87×10^{-15}	1.09×10^{-13}	34	4.26×10^{-12}	3.8×10^{-14}	8.53×10^{-13}
PP229	770	73^{+41}_{-20}	61	460	750	0.5144	385.8	22	1.02×10^{-12}	6.33×10^{-15}	1.42×10^{-13}	37	4.82×10^{-12}	4.65×10^{-14}	1.045×10^{-12}
PP225	986	70^{+36}_{-20}	56	450	650	0.416	270.4	23	6.2×10^{-13}	3.79×10^{-15}	8.37×10^{-14}	38	2.87×10^{-12}	2.73×10^{-14}	6.04×10^{-13}
PP749	942	46^{+22}_{-12}	34	380	450	0.2032	91.44	32	8.33×10^{-14}	5.07×10^{-16}	9.66×10^{-15}	50	3.32×10^{-13}	3.03×10^{-15}	5.77×10^{-14}

These data were used to calculate differential stress (Twiss, 1977; Stipp and Tullis, 2003) and strain rate (Paterson and Luan, 1990; Luan and Paterson, 1992; Hirth et al., 2001).

East–West oriented flow within the Vepor basement may be a pure shear deformation on the regional scale, which is accommodated by local conjugate simple shear zones operating on sample or even aggregate scale (Fig. 13).

6.2. Contrasting deformation pattern within the Vepor Unit

The East–West horizontal ductile flow in the Vepor Unit during D_{A1} contrasts, both, geometrically and kinematically, with the deformation of the adjacent southern Gemer and northern Tatra Units. The Cretaceous North–South shortening of the Central West Carpathians (CWC), described within the southerly supra-structural Gemer Unit and the Tatro-Fatric domain in the north (Lexa et al., 2003; Plašienka, 1995, 2003), is associated with the crustal-scale thrust sheet stacking (Tomek, 1993; Plašienka et al., 1997). Meanwhile, the low-viscosity Vepor Unit, being surrounded by two strongly non-coaxial crustal-scale thrust zones (Plašienka, 1993; Plašienka, 2003), experience coaxial orogen-parallel stretching described in this work. The orogen-parallel stretching has been documented in internal domains of many continental collisional systems and is often termed "orogen-parallel extension or lateral escape" (e.g. Ellis and Watkinson, 1987 in the Caledonides, Burg et al., 1994 in the European Variscides and Dewey et al., 1988 in the Tibetan plateau).

Orogen-parallel extension is commonly seen as associated with syn-convergent exhumation of deeply buried crustal rocks (e.g. Selverstone, 1988; Ratschbacher et al., 1991a,b; Mancktelow and Pavlis, 1994; Janák et al., 2001; Fügenschuh and Schmid, 2005). However, in the Vepor basement the deformation fabric S_{A1} is associated with an increase in pressure and temperature, suggesting that the orogen-parallel flow has occurred contemporaneously with burial (Jeřábek et al., in press).

Recently, Indares et al. (2000) described orogen-parallel stretching perpendicular to general thrusting in rheologically weaker units bounded by strong thrust sheets. These authors suggest that the lateral escape is connected to ductility contrasts between adjacent thrust slices. In agreement with this model, the Vepor Unit may be considered as the weak part of the CWC stack due to the reaction softening and the P–T increase related to its underthrusting beneath the Gemer Unit. However, the Indares et al. (2000) model does not solve the commonly criticised space problem related to lateral escape tectonics. This issue is thoroughly discussed by Seyferth and Henk (2004) who suggest that the orogen-parallel extension is intimately related to continental collision and occurs contemporaneously with convergence. In their numerical model, the lateral extrusion occurs in areas where the collision zone adjoins a weakly constrained lateral foreland (unconfined lateral boundary condition), which is only balanced by lithospheric pressure. Importantly, the Vepor – Gemer stack represents an integral part of an Eastern Alpine Cretaceous subduction – collision system, which was extruded from the Alpine domain during Cenozoic (Schmid et al., 2004). Therefore, the boundary conditions of the Early Cretaceous convergent system remain poorly constrained and the existence of unconfined eastern Alpine-Carpathian margin can be considered as a possible hypothesis (Frank and Schlager, 2006).

The last stage of the North–South convergence of the CWC recorded by the second Alpine deformation D_{A2} within the Vepor Unit is seen as large scale folding of the subhorizontal deformation fabric S_{A1} resulting in heterogeneous exhumation of the deep Vepor basement (Jeřábek et al., in press). The observed variations in differential stresses and P–T conditions at the present erosion level are most probably related to passive exhumation of orogenic fabric S_{A1} related to folding.

The D_{A2} folding event is responsible for the development of the third and lowest temperature quartz microstructure with discrete shear surfaces displaying low temperature recrystallization of quartz. These structures may be associated with the late stages of exhumation, when the tectonic denudation of the Gemer Unit occurred via low angle detachment shearing at the contact between the Vepor and Gemer Units (Hók et al., 1993; Plašienka, 1993; Plašienka et al., 1999; Janák et al., 2001).

6.3. Strain rates, temperatures and quartz microstructures in the Vepor Unit

With increasing deformation and metamorphic transformation of the granitoids the reacting products form interconnected weak layers (Handy, 1990), which progressively controls the deformation of the Král'ova Hol'a Complex. At the same time, the quartz microstructure is approximately constant, depending only on the increase of temperature towards the structural footwall. The question arises whether the metamorphic assemblage and especially the garnet zoning used for temperature estimates occurs coevally with the deformation of quartz. The linkage between S_{A1} and burial instead of exhumation is supported by: (1) the mineral assemblage of the interconnected weak layers (S_{A1}) consisting of phengitic muscovite, neocrystallized albite, biotite in equilibrium with chlorite and small garnet, which define peak P–T conditions (Jeřábek et al., in press); and (2) the absence of substantial low-temperature overprint of S_{A1} quartz microstructures as well as of low-grade reactivation of the matrix. Furthermore, the lack of annealing and relative uniformity of quartz microstructure suggests rapid transition from burial to exhumation without significant reactivation of the syn-burial fabrics, respectively.

The D_{A1} quartz microstructures in the structurally higher central and eastern parts of the Král'ova Hol'a Complex show SGR dislocation creep while the Easternmost samples suggest a near-transition to low temperature BLG creep. At natural conditions and strain rates of $\sim 10^{-12}\,s^{-1}$, the lower temperature limit of the SGR dislocation creep is expected at around 400 °C (Stipp et al., 2002a,b). In contrast, the higher temperature D_{A1} quartz microstructure in the structurally lower western part of the Král'ova Hol'a Complex shows a contribution of high temperature GBM indicating a transitional regime between SGR and GBM. Stipp et al. (2002a,b) estimate that the transition between SGR and GBM dislocation creep at

strain rates of $\sim 10^{-12}\ s^{-1}$ occurs between 490 and 530 °C. The temperature of the SGR dislocation creep in the Král'ova Hol'a Complex is estimated to be between 380 °C and 480 °C, approximately. These temperatures are lower than those of Stipp et al. (2002b) and can be explained by lower strain rates (Fig. 16).

In order to define the limits of the three dislocation creep regimes, we compare our data with published data of Hirth and Tullis (1992), Dunlap et al. (1997) and Stipp et al. (2002b) (Fig. 16). Following Stipp et al. (2002a), the boundaries between the three dislocation creep regimes in the log strain rate versus homologous temperature diagram (Fig. 16) are represented by two parallel lines connecting the naturally constrained limits of the three dislocation creep regimes (Ruby Gap Duplex of Dunlap et al., 1997; Eastern Tonale mylonite zone of Stipp et al., 2002b) with experimentally derived limits of Hirth and Tullis (1992). The slope of the boundary lines depends on the choice of flow laws, nevertheless those of Paterson and Luan (1990) and Hirth et al. (2001) yield the best correlation between the naturally and experimentally determined limits (dashed lines in Fig. 16). Fig. 16 shows that for these flow laws and for the Twiss (1977) and Stipp and Tullis (2003) piezometers, the regime boundaries of the Král'ova Hol'a Complex are in a good agreement with published data (Hirth and Tullis, 1992; Dunlap et al., 1997; Stipp et al., 2002b).

For given temperatures, pressures and stresses in the Král'ova Hol'a Complex only three combinations of piezometers and flow laws (Twiss, 1977 and Hirth et al., 2001; Twiss, 1977 and Paterson and Luan, 1990; Stipp and Tullis, 2003 and Paterson and Luan, 1990) are in a good agreement with the extent of subgrain rotation recrystallization dominated dislocation creep (Fig. 16). Using these combinations, the strain rate estimates for the Král'ova Hol'a Complex granitoids during D_{A1} range between 9×10^{-12} and $6 \times 10^{-14}\ s^{-1}$.

6.4. Strain rate gradients as a function of material properties

The calculated strain rates indicate an increase in the deformation rate towards the structural footwall of up to 1.5 orders

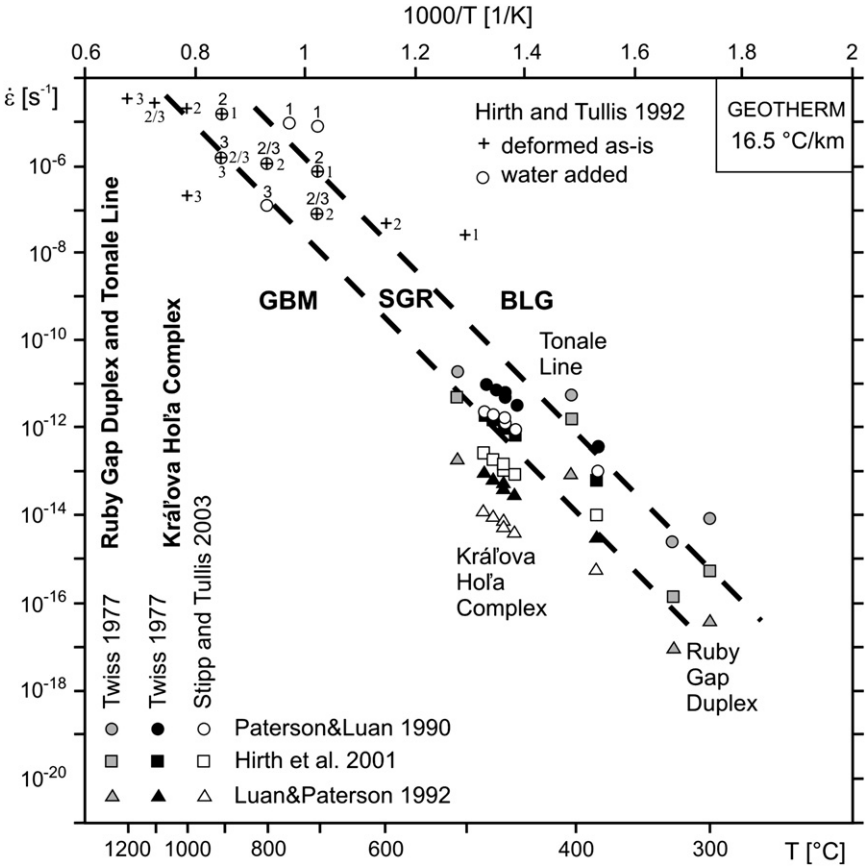

Fig. 16. Strain rate versus temperature diagram after Stipp et al. (2002a). The diagram shows experimental data of Hirth and Tullis (1992), natural data from the Ruby Gap Duplex (Dunlap et al., 1997) and Tonale Line (Stipp et al., 2002b), showing the limits of the three dislocation creep regimes, and natural data from the Král'ova Hol'a Complex (this study) covering the extent of the subgrain rotation recrystallization. The deformation temperatures are taken from Dunlap et al. (1997), Stipp et al. (2002a) and Jeřábek et al. (in press) and the stresses were obtained by piezometer of Twiss (1977) and Stipp and Tullis (2003). All the data have been normalized to water fugacities at pressures following the geothermal gradient of 16.5 °C/km determined for the Vepor Unit (Jeřábek et al., in press). The natural strain rates have been calculated from three different flow laws (Paterson and Luan, 1990; Luan and Paterson, 1992; Hirth et al., 2001). The experimental data of Hirth and Tullis (1992) are labeled by numbers indicating experimental dislocation creep regime. The dashed lines show limits of the three recrystallization mechanisms dominated by bulging recrystallization (BLG), subgrain rotation recrystallization (SGR) and grain boundary migration recrystallization (GBM) (see text for discussion).

of magnitude (Table 2, Fig. 16). With the exception of the Ruby Gap Duplex (Dunlap et al., 1997), an increase in strain rate with increasing temperature has been reported in most of the previous studies on natural mylonites (Hacker et al., 1990, 1992; Stöckhert et al., 1999; Zulauf, 2001; Stipp et al., 2002a). Such strain rate gradient can be explained by material properties indicating a temperature dependent viscosity. On the other hand, deformation partitioning can lead to similar effect by assuming its greater significance in lower temperatures. In the Král'ova Hol'a Complex granitoids, the proportion of newly formed sericitic muscovite increases towards lower temperatures (Fig. 7) enhancing deformation partitioning (Shea and Kronenberg, 1993; Holyoke and Tullis, 2006). In addition, the weak and almost random textures of neocrystallized albite grains (Fig. 9) indicate important contribution of diffusion creep causing a general mechanical weakness of the plagioclase-mica rich matrix (Stünitz and Fitz Gerald, 1993). The predominance of mechanically weak mica bands and recrystallized plagioclase matrix suggest that quartz becomes a relatively stronger mineral in greenschist granitoid mylonites (Handy, 1990). As a consequence, lower flow stresses and lower strain rates may be recorded by the recrystallized quartz in the granitoids deformed at lower temperatures. Thus the difference in strain rate along vertical section of the Král'ova Hol'a Complex is probably related to combined effect of decreasing viscosity towards higher temperatures as well as increasing deformation partitioning towards lower temperatures. Generally, it should be noted that our strain rate estimates represent minimum values as the weaker matrix is supposed to accommodate strain at a faster rate than the pure quartz aggregates.

7. Conclusions

The Cretaceous subhorizontal plane strain deformation fabric in the Vepor Unit overprints the Variscan magmatic and high grade fabrics and exhibits orogen-parallel stretching with regionally variable senses of shear. It is suggested that the regional pure shear geometry of this East–West orogen-parallel flow is the cumulated results of local simple shear components. The deformation occurred during progressive burial and records a process of orogen-parallel ductile spreading of the Veporic crust in between the Gemer Unit, overthrusting from the South, and Tatro-Fatric basement, underthrusting from the North. Observed metamorphic gradients across the Vepor Unit are interpreted to result from later folding and heterogeneous exhumation of the orogen-parallel deformation fabric.

Deformation microstructures of quartzo-feldspathic rocks, related to the orogen-parallel flow in the Vepor Unit, develop along a metamorphic gradient indicating an increase in P–T conditions from 380 to 480 °C towards the structural footwall. The recrystallization of quartz takes place across the field of rotation recrystallization accommodated dislocation creep, permitting the strain rate/temperature/microstructure calibration, which is consistent with previous calibrations. Palaeopiezometry of recrystallized quartz in conjunction with P–T estimates yield strain rates ranging from 9×10^{-12} to 6×10^{-14} s^{-1}. The calculated strain rates increase with increasing temperature towards the structural footwall as a result of combined effect of temperature dependent viscosity and deformation partitioning in granitoids deformed at lower temperatures.

Acknowledgements

This work was supported by Research Grants of the Czech Science Foundation (GACR 205/03/1490) and Charles University Science Foundation (GAUK 373/2004), and by the Ministry of Education, Youth and Sports of the Czech Republic project No. MSM0021620855. M. Machek is thanked for field work participation and M. Stipp for helpful discussions. K. Kanawaga and D. Plašienka are thanked for careful and constructive reviews and C. Passchier is thanked for his editorial work. G.K.CH. is thanked for inspiration.

References

Bezák, V., Jacko, S., Janák, M., Ledru, P., Petrík, I., Vozárová, A., 1997. Main Hercynian lithotectonic units of the Western Carpathians. In: Grecula, P., Hovorka, D., Putiš, M. (Eds.), Geological Evolution of the Western Carpathians. Mineralia Slovaca Corporation, Geocomplex, Bratislava, pp. 261–268.

Bibikova, E.V., Cambel, B., Korikovsky, S.P., Broska, I., Gracheva, T.V., Makarov, V.A., Arakeljants, M.M., 1988. U-Pb and K-Ar isotopic dating of Sinec (Rimavica) granites (Kohút zone of Veporides). Geologický Zborník Geologica Carpathica 39, 147–157.

Bibikova, E.V., Korikovsky, S.P., Putiš, M., Broska, I., Goltzman, Y.V., Arakeliants, M., 1990. U-Pb, Rb-Sr and K-Ar dating of Sihla tonalites of Vepor Pluton (Western Carpathian Mts.). Geologický Zborník Geologica Carpathica 41, 427–436.

Biely, A., 1964. Ueber die "Veporiden". Geologický Zborník Geologica Carpathica 15, 263–266.

Burg, J.P., Vandendriessche, J., Brun, J.P., 1994. Syn-thickening to post-thickening extension – mode and consequences. Comptes Rendus de l'Academie des Sciences Serie II 319, 1019–1032.

Christie, J.M., Ord, A., Koch, P.S., 1980. Relationship between recrystallized grain size and flow stress in experimentally deformed quartzite. EOS Transactions 61, 377.

Connolly, J.A.D., 2005. Computation of phase equilibria by linear programming: a tool for geodynamic modeling and its application to subduction zone decarbonation. Earth and Planetary Science Letters 236, 524–541.

Dewey, J.F., Shackleton, R.M., Chang, C.F., Sun, Y.Y., 1988. The tectonic evolution of the Tibetan plateau. Philosophical Transactions of the Royal Society of London Series A-Mathematical Physical and Engineering Sciences 327, 379–413.

Dunlap, W.J., Hirth, G., Teyssier, C., 1997. Thermomechanical evolution of a ductile duplex. Tectonics 16, 983–1000.

Ellis, M., Watkinson, A.J., 1987. Orogen-parallel extension and oblique tectonics – the relation between stretching lineations and relative plate motions. Geology 15, 1022–1026.

Faryad, S.W., 1991. Pre-Alpine metamorphic events in Gemericum. Mineralia Slovaca 23, 395–402.

Faryad, S.W., 1995. Phase petrology and P–T conditions of mafic blueschists from the Meliata unit, West Carpathians, Slovakia. Journal of Metamorphic Geology 13, 701–714.

Faryad, S.W., 1997. Metamorphic petrology of the Early Paleozoic low-grade rocks in the Gemericum. In: Grecula, P., Hovorka, D., Putiš, M. (Eds.), Geological Evolution of the Western Carpathians. Mineralia Slovaca Corporation, Geocomplex, Bratislava, pp. 309–314.

Faryad, S.W., Henjes-Kunst, F., 1997. Petrological and K-Ar and Ar-40-Ar-39 age constraints for the tectonothermal evolution of the high-pressure Meliata unit, Western Carpathians (Slovakia). Tectonophysics 280, 141–156.

Fliervoet, T.F., White, S.H., Drury, M.R., 1997. Evidence for dominant grain-boundary sliding deformation in greenschist- and amphibolite-grade polymineralic ultramylonites from the Redbank Deformed Zone, Central Australia. Journal of Structural Geology 19, 1495–1520.

Frank, W., Schlager, W., 2006. Jurassic strike slip versus subduction in the Eastern Alps. International Journal of Earth Sciences 95, 431–450.

Fügenschuh, B., Schmid, S.M., 2005. Age and significance of core complex formation in a very curved orogen: evidence from fission track studies in the South Carpathians (Romania). Tectonophysics 404, 33–53.

Gleason, G.C., Tullis, J., 1993. Improving flow laws and piezometers for quartz and feldspar aggregates. Geophysical Research Letters 20, 2111–2114.

Gleason, G.C., Tullis, J., 1995. A flow law for dislocation creep of quartz aggregates determined with the molten-salt cell. Tectonophysics 247, 1–23.

Hacker, B.R., Yin, A., Christie, J.M., Snoke, A.W., 1990. Differential stress, strain rate, and temperatures of mylonitization in the Ruby Mountains, Nevada – implications for the rate and duration of uplift. Journal of Geophysical Research 95, 8569–8580.

Hacker, B.R., Yin, A., Christie, J.M., Davis, G.A., 1992. Stress magnitude, strain rate, and rheology of extended middle continental-crust inferred from quartz grain sizes in the Whipple Mountains, California. Tectonics 11, 36–46.

Handy, M.R., 1990. The solid-state flow of polymineralic rocks. Journal of Geophysical Research 95, 8647–8661.

Heilbronner, R., 2000. Automatic grain boundary detection and grain size analysis using polarization micrographs or orientation images. Journal of Structural Geology 22, 969–981.

Heilbronner, R., Tullis, J., 2002. The effect of static annealing on microstructure and crystallographic preferred orientations of quartzites experimentally deformed in axial compression and shear. In: de Meer, S., Drury, M.R., de Bresser, J.H.P., Pennock, G.M. (Eds.), Deformation Mechanisms, Rheology and Tectonics: Current Status and Future Perspectives. Special Publications, vol. 200. Geological Society, London, pp. 191–218.

Hippertt, J.F., 1998. Breakdown of feldspar, volume gain and lateral mass transfer during mylonitization of granitoid in a low metamorphic grade shear zone. Journal of Structural Geology 20, 175–193.

Hirth, G., Tullis, J., 1992. Dislocation creep regimes in quartz aggregates. Journal of Structural Geology 14, 145–159.

Hirth, G., Teyssier, C., Dunlap, W.J., 2001. An evaluation of quartzite flow laws based on comparisons between experimentally and naturally deformed rocks. International Journal of Earth Sciences 90, 77–87.

Hók, J., Kováč, P., Madarás, J., 1993. Extenzná tektonika západného úseku styčnej zóny gemerika a veporika Translated Title: Extensional tectonics of the western part of the contact area between Veporicum and Gemericum. Mineralia Slovaca 25, 172–176.

Holyoke, C.W., Tullis, J., 2006. Mechanisms of weak phase interconnection and the effects of phase strength contrast on fabric development. Journal of Structural Geology 28, 621–640.

Hrouda, F., Putiš, M., Madarás, J., 2002. The Alpine overprints of the magnetic fabrics in the basement and cover rocks of the Veporic Unit (Western Carpathians, Slovakia). Tectonophysics 359, 271–288.

Indares, A., Dunning, G., Cox, R., 2000. Tectono-thermal evolution of deep crust in a Mesoproterozoic continental collision setting: the Manicouagan example. Canadian Journal of Earth Sciences 37, 325–340.

Jacko, S., Sasvari, T., Zacharov, M., Schmidt, R., Vozár, J., 1996. Contrasting styles of Alpine deformations at the eastern part of the Veporicum and Gemericum units, Western Carpathians. Slovak Geological Magazine 2, 151–164.

Janák, M., 1994. Variscan uplift of the crystalline basement, Tatra Mts., Central Western Carpathians: evidence from 40Ar/39Ar laser probe dating of biotite and P–T–t paths. Geologica Carpathica 45, 293–300.

Janák, M., Plašienka, D., Frey, M., Cosca, M., Schmidt, S.T., Lupták, B., Méres, Š., 2001. Cretaceous evolution of a metamorphic core complex, the Veporic unit, Western Carpathians (Slovakia): P–T conditions and in situ Ar-40/Ar-39 UV laser probe dating of metapelites. Journal of Metamorphic Geology 19, 197–216.

Jeřábek, P., Faryad, S.W., Schulmann, K., Lexa, O., Tajčmanová, L., (in press) Alpine burial and heterogeneous exhumation of Variscan crust in the West Carpathians: insight from thermodynamic and argon diffusion modelling. Journal of the Geological Society.

Ji, S.C., Mainprice, D., 1988. Natural deformation fabrics of plagioclase – implications for slip systems and seismic anisotropy. Tectonophysics 147, 145–163.

Klinec, A., 1966. K problémom stavby a vzniku veporského kryštalinika Translated Title: on the structure and evolution of the Veporic crystalline unit. Zborník Geologických Vied 6, 7–28.

Kohlstedt, D.L., Evans, B., Mackwell, S.J., 1995. Strength of the lithosphere – constraints imposed by laboratory experiments. Journal of Geophysical Research 100, 17587–17602.

Koch, P.S., 1983. Rheology and microstructures of experimentally deformed quartz aggregates. PhD thesis, University of California.

Koroknai, B., Horvath, P., Balogh, K., Dunkl, I., 2001. Alpine metamorphic evolution and cooling history of the Veporic basement in northern Hungary: new petrological and geochronological constraints. International Journal of Earth Sciences 90, 740–751.

Kováčik, M., Král', J., Maluski, H., 1996. Alpinský metamorfný a termochronologický vývoj juhoveporických predalpínskych metamorfitov Translated Title: Metamorphic rocks in the Southern Veporicum basement: their Alpine metamorphism and thermochronologic evolution. Mineralia Slovaca 28, 185–202.

Král', J., Frank, W., Bezák, V., 1996. $^{40}Ar/^{39}Ar$ spektra z amfibolu amfibolickych hornin veporika Translated Title: The $^{40}Ar/^{39}Ar$ spectra of hornblende from the amphibole-bearing rocks of the Veporic unit. Mineralia Slovaca 28, 501–513.

Krist, E., Korikovsky, S.P., Putiš, M., Janák, M., Faryad, S.W., 1992. Geology and Petrology of Metamorphic Rocks of the Western Carpathian Crystalline Complexes. Comenius University Press, Bratislava.

Kruse, R., Stünitz, H., Kunze, K., 2001. Dynamic recrystallization processes in plagioclase porphyroclasts. Journal of Structural Geology 23, 1781–1802.

Kurz, W., Unzog, W., Neubauer, F., Genser, J., 2001. Evolution of quartz microstructures and textures during polyphase deformation within the Tauern Window (Eastern Alps). International Journal of Earth Sciences 90, 361–378.

Kurz, W., Fritz, H., Tenczer, V., Unzog, W., 2002. Tectonometamorphic evolution of the Koralm Complex (Eastern Alps): constraints from microstructures and textures of the 'Plattengneis' shear zone. Journal of Structural Geology 24, 1957–1970.

Lexa, O., 2003. Numerical approaches in structural and microstructural analysis. PhD thesis, Charles University.

Lexa, O., Schulmann, K., Ježek, J., 2003. Cretaceous collision and indentation in the West Carpathians: view based on structural analysis and numerical modeling. Tectonics 22. art. no.1066.

Lister, G.S., Hobbs, B.E., 1980. The simulation of fabric development during plastic-deformation and its application to quartzite – the influence of deformation history. Journal of Structural Geology 2, 355–370.

Lister, G.S., Williams, P.F., 1979. Fabric development in shear zones – theoretical controls and observed phenomena. Journal of Structural Geology 1, 283–297.

Lobkowicz, M., Schulmann, K., Melka, R., 1998. Variscan deformation, microstructural zonation and extensional exhumation of the Moravian Cadomian basement. Geodinamica Acta 11, 119–137.

Luan, F.C., Paterson, M.S., 1992. Preparation and deformation of synthetic aggregates of quartz. Journal of Geophysical Research 97, 301–320.

Lupták, B., Janák, M., Plašienka, D., Schmidt, S.T., Frey, M., 2000. Chloritoid-kyanite schists from the Veporic unit, Western Carpathians, Slovakia: implications for Alpine (Cretaceous) metamorphism. Schweizerische Mineralogische und Petrographische Mitteilungen 80, 213–223.

Lupták, B., Janák, M., Plašienka, D., Schmidt, S.T., 2003. Alpine low grade metamorphism of the Permian-Triassic sedimentary rocks from the Veporic superunit, Western Carpathians: phyllosilicate composition and ''crystallinity'' data. Geologica Carpathica 54, 367–375.

Maluski, H., Rajlich, P., Matte, P., 1993. $^{40}Ar - {}^{39}Ar$ dating of the Inner Carpathians Variscan basement and Alpine mylonitic overprinting. Tectonophysics 223, 313–337.

Mancktelow, N.S., Pavlis, T.L., 1994. Fold-fault relationships in low-angle detachment systems. Tectonics 13, 668–685.

Mares, V.M., Kronenberg, A.K., 1993. Experimental deformation of muscovite. Journal of Structural Geology 15, 1061–1075.

Mariani, E., Brodie, K.H., Rutter, E.H., 2006. Experimental deformation of muscovite shear zones at high temperatures under hydrothermal conditions and the strength of phyllosilicate-bearing faults in nature. Journal of Structural Geology 28, 1569–1587.

Mercier, J.C., Anderson, D.A., Carter, N.L., 1977. Stress in the lithosphere; inferences from steady state flow of rocks. Pure and Applied Geophysics 115, 199–226.

Méres, Š., Hovorka, D., 1991. Alpine metamorphic recrystallization of the pre-Carboniferous metapelites of the Kohút crystalline complex (the Western Carpathians). Mineralia Slovaca 23, 435–442.

Michalko, J., Bezák, V., Hraško, L., Král', J., Huhma, H., Mantari, I., Vaasjoki, M., Broska, I., Határ, J., 1998. U/Pb zircon data of the Veporic granitoids (Western Carpathians). Krystalinikum 24, 91–104.

Newman, J., Lamb, W.M., Drury, M.R., Vissers, R.L.M., 1999. Deformation processes in a peridotite shear zone: reaction-softening by an H2O-deficient, continuous net transfer reaction. Tectonophysics 303, 193–222.

Padmanabhan, K.A., Davies, G.J., 1980. Superplasticity. Springer, New York.

Panozzo Heilbronner, R., Pauli, C., 1993. Integrated spatial and orientation analysis of quartz c-axes by computer-aided microscopy. Journal of Structural Geology 15, 369–382.

Paterson, M.S., 1989. The interaction of water with quartz and its influence in dislocation flow – an overview. In: Karato, S.I., Toriumi, M. (Eds.), Rheology of Solids and of the Earth. Oxford University Press, Oxford, pp. 107–142.

Paterson, M.S., Luan, F.C., 1990. Quartzite rheology under geological conditions. In: Knipe, R.J., Rutter, E.H. (Eds.), Deformation Mechanisms, Rheology and Tectonics. Special Publications, vol. 54. Geological Society, London, pp. 299–307.

Petrasová, K., Faryad, S.W., Jeřábek, P., Žáčková, E., 2007. Origin and metamorphic evolution of magnesite-talc and adjacent rocks near Gemerská Poloma, Slovak Republic. Journal of Geosciences 52, 125–132.

Plašienka, D., 1993. Structural pattern and partitioning of deformation in the Veporic Foederata cover unit (Central Western Carpathians). In: Rakús, M., Vozár, J. (Eds.), Geodynamic Model and Deep Structure of the Western Carpathians. Geologický Ústav Dionýza Štúra, Bratislava, pp. 269–277.

Plašienka, D., 1995. Passive and active margin history of the northern Tatricum (Western Carpathians, Slovakia). Geologische Rundschau 84, 748–760.

Plašienka, D., 2003. Development of basement-involved fold and thrust structures exemplified by the Tatric-Fatric-Veporic nappe system of the Western Carpathians (Slovakia). Geodinamica Acta 16, 21–38.

Plašienka, D., Grecula, P., Putiš, M., Kováč, M., Hovorka, D., 1997. Evolution and structure of the Western Carpathians: an overview. In: Rakús, M., Vozár, J. (Eds.), Geological Evolution of the Western Carpathians. Mineralia Slovaca Corporation, Geocomplex, Bratislava, pp. 1–24.

Plašienka, D., Janák, M., Lupták, B., Milovský, R., Frey, M., 1999. Kinematics and metamorphism of a Cretaceous core complex: the Veporic unit of the Western Carpathians. Physics and Chemistry of the Earth, part a – Solid Earth and Geodesy 24, 651–658.

Poirier, J.P., Guillope, M., 1979. Deformation induced recrystallization of minerals. In: Nicolas, A., Darot, M., Willaime, C. (Eds.), Mecanismes de Deformation des Mineraux et des Roches. Bulletin de Mineralogie, vol. 102. Masson, Paris, pp. 67–74.

Post, A.D., Tullis, J., Yund, R.A., 1996. Effects of chemical environment on dislocation creep of quartzite. Journal of Geophysical Research 101, 22143–22155.

Prior, D.J., Knipe, R.J., Handy, M.R., 1990. Estimates of the rates of microstructural change in mylonites. In: Knipe, R.J., Rutter, E.H. (Eds.), Deformation Mechanisms, Rheology and Tectonics. Special Publications, vol. 54. Geological Society, London, pp. 309–319.

Putiš, M., Unzog, W., Wallbrecher, E., Fritz, H., 1997. Mylonitization and chemical mass-transfer in granitoid rocks of the Vepor pluton near the Cretaceous Pohorelá thrust (Veporic unit, central Western Carpathians). In: Grecula, P., Hovorka, D., Putiš, M. (Eds.), Geological Evolution of the Western Carpathians. Mineralia Slovaca Corporation, Geocomplex, Bratislava, pp. 197–214.

Ramsay, J.G., 1967. Folding and Fracturing of Rocks. McGraw-Hill, New York.

Ranalli, G., 1984. Grain size distribution and flow stress in tectonites. Journal of Structural Geology 6, 443–447.

Ratschbacher, L., Merle, O., Davy, P., Cobbold, P., 1991a. Lateral extrusion in the Eastern Alps 1 – boundary conditions and experiments scaled for gravity. Tectonics 10, 245–256.

Ratschbacher, L., Frisch, W., Linzer, H.G., Merle, O., 1991b. Lateral extrusion in the Eastern Alps 2 – structural analysis. Tectonics 10, 257–271.

Rutter, E.H., Casey, M., Burlini, L., 1994. Preferred crystallographic orientation development during the plastic and superplastic flow of calcite rocks. Journal of Structural Geology 16, 1431–1446.

Scheidegger, A.E., 1965. On the statistics of the orientation of bedding planes, grain axes, and similar sedimentological data. US Geological Survey Professional Paper (525-C). 164–167.

Schmid, S.M., Casey, M., 1986. Complete fabric analysis of some commonly observed quartz [c]-axis patterns. In: Hobbs, B.E., Heard, H.C. (Eds.), Mineral and Rock Deformation: Laboratory Studies; the Paterson Volume. Geophysical Monograph, vol. 36. American Geophysical Union, Washington DC, pp. 263–286.

Schmid, S.M., Fugenschuh, B., Kissling, E., Schuster, R., 2004. Tectonic map and overall architecture of the Alpine orogen. Eclogae Geologicae Helvetiae 97, 93–117.

Selverstone, J., 1988. Evidence for east-west crustal extension in the Eastern Alps – implications for the unroofing history of the Tauern Window. Tectonics 7, 87–105.

Seyferth, M., Henk, A., 2004. Syn-convergent exhumation and lateral extrusion in continental collision zones – insights from three-dimensional numerical models. Tectonophysics 382, 1–29.

Shea, W.T., Kronenberg, A.K., 1993. Strength and anisotropy of foliated rocks with varied mica contents. Journal of Structural Geology 15, 1097–1121.

Siegl, K., 1982. Structure of the Vepor pluton (West Carpathians). Geologica Carpathica 33, 171–175.

Siman, P., Johan, V., Ledru, P., Bezák, V., Madarás, J., 1996. Deformation and p-T conditions estimated in "layered migmatites" from southern part of Veporicum crystalline basement (Western Carpathians, Slovakia). Slovak Geological Magazine 3, 209–213.

Simpson, C., Schmid, S.M., 1983. An evaluation of criteria to deduce the sense of movement in sheared rocks. Geological Society of America Bulletin 94, 1281–1288.

Stipp, M., Tullis, J., 2003. The recrystallized grain size piezometer for quartz. Geophysical Research Letters 30. art. no. 2088.

Stipp, M., Stünitz, H., Heilbronner, R., Schmid, S.M., 2002a. Dynamic recrystallization of quartz: correlation between natural and experimental conditions. In: de Meer, S., Drury, M.R., de Bresser, J.H.P., Pennock, G.M. (Eds.), Deformation Mechanisms, Rheology and Tectonics: Current Status and Future Perspectives. Special Publications, vol. 200. Geological Society, London, pp. 171–190.

Stipp, M., Stünitz, H., Heilbronner, R., Schmid, S.M., 2002b. The eastern Tonale fault zone: a 'natural laboratory' for crystal plastic deformation of quartz over a temperature range from 250 to 700 °C. Journal of Structural Geology 24, 1861–1884.

Stipp, M., Fügenschuh, B., Gromet, L.P., Stünitz, H., Schmid, S.M., 2004. Contemporaneous plutonism and strike-slip faulting: A case study from the Tonale fault zone north of the Adamello pluton (Italian Alps). Tectonics 23. art. no. 3004.

Stöckhert, B., Brix, M.R., Kleinschrodt, R., Hurford, A.J., Wirth, R., 1999. Thermochronometry and microstructures of quartz – a comparison with experimental flow laws and predictions on the temperature of the brittle-plastic transition. Journal of Structural Geology 21, 351–369.

Stünitz, H., 1998. Syndeformational recrystallization – dynamic or compositionally induced? Contributions to Mineralogy and Petrology 131, 219–236.

Stünitz, H., Fitz Gerald, J.D., 1993. Deformation of granitoids at low metamorphic grade 2 – granular flow in albite-rich mylonites. Tectonophysics 221, 299–324.

Stünitz, H., Fitz Gerald, J.D., Tullis, J., 2003. Dislocation generation, slip systems, and dynamic recrystallization in experimentally deformed plagioclase single crystals. Tectonophysics 372, 215–233.

Tödheide, K., 1972. Water at high temperature and pressure. In: Franks, F. (Ed.), Water: A Comprehensive Treatise, vol. 1. Plenum Press, New York, pp. 463–514.

Tomek, C., 1993. Deep-crustal structure beneath the Central and Inner West Carpathians. Tectonophysics 226, 417–431.

Tullis, J., Yund, R.A., 1985. Dynamic recrystallization of feldspar – a mechanism for ductile shear zone formation. Geology 13, 238–241.

Twiss, R.J., 1977. Theory and applicability of a recrystallized grain size paleopiezometer. Pure and Applied Geophysics 115, 227–244.

Urai, J.L., Means, W.D., Lister, G.S., 1986. Dynamic recrystallization of minerals. In: Hobbs, B.E., Heard, H.C. (Eds.), Mineral and Rock Deformation: Laboratory Studies; the Paterson Volume. Geophysical Monograph, vol. 36. American Geophysical Union, Washington DC, pp. 161–199.

Vrána, S., 1980. Newly-formed Alpine garnets in metagranitoids of the Veporides in relation to the structure of the Central zone of the West Carpathians. Časopis pro Mineralogii a Geologii 25, 41–54.

White, S., 1979. Grain and sub-grain size variations across a mylonite zone. Contributions to Mineralogy and Petrology 70, 193–202.

Zulauf, G., 2001. Structural style, deformation mechanisms and paleodifferential stress along an exposed crustal section: constraints on the ;rheology of quartzofeldspathic rocks at supra- and infrastructural levels (Bohemian Massif). Tectonophysics 332, 211–237.